This is a preprint, the final version is subject to change, of the American Mineralogist (MSA)
Cite as Authors (Year) Title. American Mineralogist, in press.
(DOI will not work until issue is live.) DOI: http://dx.doi.org/10.2138/am-2016-5118

REVISION 2

Fluids in the crust during regional metamorphism: Forty years in the Waterville limestone

JOHN M. FERRY*

Department of Earth and Planetary Sciences, Johns Hopkins University, Baltimore, Maryland 21218, U.S.A.

*E-Mail: jferry@jhu.edu

ABSTRACT

Research over the last four decades on carbonate rocks of the Waterville limestone, Maine, U.S.A., has contributed to the development of both concepts and methodologies for understanding fluid-rock interaction during regional metamorphism, including: (a) buffering of fluid composition by mineral reactions, (b) infiltration of carbonate rocks by aqueous fluids, (c) petrologic fluid-rock ratios, (d) infiltration-driven metamorphism, (e) one- and two-dimensional continuum models for coupled fluid flow and mineral reaction, (f) time-integrated fluid fluxes, and (g) channelized, horizontal fluid flow in the direction of increasing temperature within chemically isolated layers. Disagreement between the last concept and both hydrodynamic models for metamorphic fluid flow and empirical evidence for homogenization of fluid composition at a scale much larger than layer thickness motivated development of the latest models for coupled fluid flow and mineral reaction in the Waterville limestone. The new models consider a flow medium composed of layers that differ in the initial amounts and compositions of minerals, both horizontal flow in the direction of increasing temperature and vertical flow in the direction of decreasing pressure and temperature, significant but imperfect homogenization of fluid composition across layering by CO_2-H_2O interdiffusion, and infiltration by fluids that are spatially variable in composition on the km scale with CO_2 content increasing with increasing grade of metamorphism. The new models reproduce measured progress of the biotite-forming

reaction in the Waterville limestone over a range of spatial scales spanning six orders of magnitude, from differences in reaction progress of up to a factor of ~100 between adjacent cm-thick layers to the coexistence of mineral reactants and products over a distance of ~13 km parallel to the metamorphic field gradient. Results imply that the present spatial distributions of reaction progress represent a steady state achieved when rocks closely approached equilibrium with the infiltrating fluid during metamorphism. The new models resolve what for many years appeared to be fundamental discrepancies among petrologic data for regionally metamorphosed carbonate rocks, hydrodynamic models of regional metamorphism, and the length scales of mass transport of volatiles across layering by diffusion.

INTRODUCTION AND HISTORICAL BACKGROUND

Studies of decarbonation reactions and the CO_2-bearing fluids that they produce have played a vital role over the last century in development of the current understanding of metamorphism. As reviewed by Evans (2007), estimation of the *P*-*T* conditions of the equilibrium among calcite, quartz, wollastonite, and CO_2 was the first thermodynamic calculation applied to a significant problem in metamorphic petrology (Goldschmidt, 1912). Although ignoring molar volumes of the minerals and suffering from inaccurate enthalpy, entropy, and heat capacity data and an absence of *P*-*V*-*T* data and fugacity coefficients for CO_2 (Goldschmidt assumed ideal gas behavior), the calculated *P*-*T* curve, surprisingly, lies within 100 °C of one computed from a modern geochemical data base (Berman, 1988, updated 1992) over the *P* range 1000 – 10,000 atm. The result remained one of the few credible estimates of the temperatures of metamorphism for more than 30 years. From a contemporary perspective, however, the principal shortcoming in any application of Goldschmidt's calculation is that metamorphic fluids normally contain only a small mole fraction of CO_2 (X_{CO_2}).

Moving forward in Evans' (2007) review, a second milestone in the development of metamorphic petrology that emerged from study of decarbonation reactions was Bowen's (1940) naming and explication of the concept of a petrogenetic grid using 13 decarbonation reactions as an example (see also Essene, 1982). Furthermore, Bowen's remarkable paper (a) recognized that progressive metamorphism of siliceous carbonate rocks was a process of progressive decarbonation, (b) provided the first rigorous analysis of the relationship between rock composition and mineral assemblage on triangular composition diagrams in divariant regions between univariant reaction curves, and (c) made remarkable predictions about occurrences of calc-silicate minerals that could occur from infiltration of fluids during metamorphism. From a contemporary perspective, as with Goldschmidt's calculation, the principal shortcoming of applications of Bowen's petrogenetic grid is that fluids during metamorphism of siliceous carbonate rocks are rarely pure CO_2. Had Bowen known that fluids are CO_2-H_2O solutions with variable X_{CO_2} during progressive metamorphism of siliceous carbonate rocks, his puzzlement over seemingly contradictory field occurrences of wollastonite and periclase would have been easily resolved.

As additionally reviewed by Evans (2007), Greenwood's (1963) thermodynamic analysis of equilibria among minerals and CO_2-H_2O fluids solved the problem of applying calculations like Goldschmidt's and petrogenetic grids like Bowen's that assumed the presence of pure CO_2 fluid during metamorphism. Greenwood's representation of mineral-fluid equilibria on isobaric T-X_{CO_2} (or isothermal P-X_{CO_2}) diagrams allowed rigorous interpretation of mineral assemblages in metamorphosed siliceous carbonates in terms of both T (or P) and fluid composition. Greenwood's development of T-X_{CO_2} diagrams stimulated much groundbreaking research on mineral reactions and fluid-rock interaction in metamorphosed siliceous carbonate rocks. The

prediction in Greenwood (1963) that spatially variable fluid composition during metamorphism could lead to intersecting isograds was confirmed by Carmichael (1970). Theoretical representation of progressive metamorphism on T-X_{CO_2} diagrams (Greenwood, 1967) led to the prediction that fluid composition should normally be buffered by mineral reactions in carbonate-bearing rocks. The prediction was confirmed in numerous studies, initially by Hewitt (1973) in regional metamorphic rocks and most convincingly by Rice (1977a,b) in contact metamorphic rocks.

ENTER THE WATERVILLE LIMESTONE

I first visited and collected samples from the Waterville limestone in July, 1972. The initial goal was to identify and characterize a miscibility gap (or gaps) in calcic plagioclase feldspar. Feldspar compositions proved difficult to interpret (and remain so), and focus of the fieldwork quickly changed to a petrologic investigation of carbonate rocks. Over the next four plus decades, the Waterville limestone served, and continues to serve, as a natural laboratory for numerous studies of decarbonation reactions and the behavior of fluids during metamorphism.

Geologic setting

The broader geologic context of the Waterville Formation, south-central Maine, U.S.A., was established and extensively reviewed by Osberg (1968, 1979, 1988, Fig. 1). Briefly, the Waterville Formation is Silurian in depositional age and largely composed of metamorphosed interbedded shale, micaceous sandstone, and minor marl. The Waterville limestone, the focus of this paper, is a distinctive ~100-m thick member of the Waterville Formation that is marl with rare schist interbeds (<1%). The Waterville Formation was deformed and regionally metamorphosed during the Devonian Acadian Orogeny. The outcrop pattern of the Waterville

limestone is defined by isoclinally refolded recumbent folds. Lithological layering is several mm to several cm thick and, except in rarely exposed fold hinges, is everywhere nearly vertical and strikes NE-SW. Osberg (1968 and personal communication) and Ferry (1984) mapped isograds in pelitic schists based on the development of biotite, garnet, staurolite + andalusite, and sillimanite during Buchan regional metamorphism. Porphyroblasts of biotite and amphibole in the Waterville limestone crosscut foliation parallel to the axial planes of the isoclinal folds. Metamorphism therefore followed almost all deformation. At high metamorphic grades the Waterville Formation and the adjacent Vassalboro Formation were intruded by two granite plutons. Tucker et al. (2001) report a U-Pb zircon age of 378±1 Ma for the Togus pluton. The 364±3.5 Ma age of metamorphic monazite from pelites of the Waterville Formation (Wing et al., 2003) suggest that metamorphism was slightly younger than the plutonism. Based on mineral equilibria, *P* during metamorphism was ~3500 bars and *T* ranged from <400 °C in the chlorite zone to ~550 °C in the sillimanite zone.

Isograds based on the development of biotite, calcic amphibole, clinozoisite, and diopside were mapped in the Waterville limestone, thin carbonate interbeds in the normal Waterville Formation, and the Vassalboro Formation. For clarity, isograds in carbonate rocks are only illustrated for the Vassalboro Formation in Fig. 1. Mineral assemblages at five outcrops in the Waterville limestone that have been the subject of intensive research demonstrate that isograds for biotite, amphibole, clinozoisite, and diopside lie at approximately similar positions in the Waterville limestone (numbered locations, Fig. 1). (A few marl layers at location 5 contain calcic amphibole; the location is assigned to the biotite zone because the large majority of layers contain biotite but not amphibole.) Because of the simple orientation of lithologic layering in the Waterville Formation and because isograds in pelites and carbonate rocks cut across layering at a

high angle, the area offers the unusual opportunity to study fluid behavior and fluid-rock interaction in a single lithology over a wide range of grades.

Buffering of metamorphic fluid composition by mineral reactions

The first study of fluids and fluid-rock interaction in the Waterville limestone followed the lead of Hewitt (1973) in lithologically similar rocks of the Wepawaug Schist in south-central Connecticut. As in the Wepawaug Schist, reactants and products of prograde mineral reactions in marls of the Waterville limestone are spatially very widely distributed. For example, reactants and products of the biotite-forming reaction are ubiquitous between locations 7 and 5, Fig. 1, over a distance of 12.8 km parallel to the metamorphic field gradient, over a range in T of ~50 °C. In the analysis of model mineral reactions on isobaric T-X_{CO_2} diagrams, the T-X_{CO_2} path of metamorphism in the marls must have largely followed univariant reaction curves, a confirmation of Greenwood's (1967) prediction that fluid composition during metamorphism of carbonate rocks should be buffered by mineral decarbonation reactions.

Buffering of fluid composition by mineral-fluid equilibria during metamorphism of the Waterville limestone was further confirmed by calculation of layer-to-layer differences in the chemical potentials of CO_2 and H_2O (μ_{CO_2} and μ_{H_2O}) using differential thermodynamics (also known as the Gibbs method) developed by Rumble (1974, 1978) based on lectures given by J. B. Thompson, Jr. Thirty samples of the Waterville limestone were collected in 1976 along a ~100 m traverse perpendicular to layering at location 5 (Fig. 1). Small, but significant differences, in μ_{CO_2} and μ_{H_2O} of up to ~100 cal among the samples are recorded by differences in the composition of chlorite coexisting with muscovite, biotite, calcite, ankerite, quartz, plagioclase, pyrrhotite, and graphite (Ferry, 1979). The chemical potential differences require internal control of metamorphic fluid composition within rocks by mineral-fluid equilibria rather than control

imposed by external processes. Samples from the traverse have been repeatedly used for almost 40 years to develop new concepts in fluid-rock interaction during regional metamorphism and to disprove old ones. Selected data for 24 of these samples used in this study are shown in Fig. 2a.

Fluid infiltration, fluid-rock ratios, and infiltration-driven metamorphism

Amazingly, Bowen (1940, p. 262) first predicted the expected petrologic evidence for infiltration of carbonate rocks by H_2O-rich fluids during metamorphism, namely that decarbonation reactions would occur at lower metamorphic grades than expected if infiltration occurred. Hewitt (1973) first confirmed Bowen's prediction by documenting apparently higher-grade mineral assemblages at the contact between marl layers and adjacent pelites in the Wepawaug Schist compared to mineral assemblages in the interior of the marl layers. The difference was interpreted as infiltration of H_2O-rich fluid into metacarbonate rocks from surrounding pelitic schists. Hewitt further recognized that the observed prograde sequence of decarbonation reactions required infiltration of carbonate rocks by H_2O-rich fluid because T-X_{CO_2} paths defined by the reactions followed a model isobaric univariant reaction curve until a reactant mineral was exhausted and then jumped isothermally to the adjacent reaction curve at lower X_{CO_2}. Similar behavior was documented for metamorphism of the Waterville limestone by the formation of clinozoisite. The mineral reaction by which clinozoisite formed has a steep negative slope at low X_{CO_2} on a T-X_{CO_2} diagram and can only be accessed by a prograde T-X_{CO_2} path that has a significant horizontal component in the direction of decreasing X_{CO_2}.

Inspired by Taylor's use of oxygen isotope fluid-rock ratios to document infiltration of meteoric water in hydrothermal systems (Taylor, 1974, 1977, 1978), a method to calculate fluid-rock ratios based on decarbonation reactions was developed. The first published petrologic fluid-rock ratios were based on data for carbonate rocks from the Waterville Formation (Ferry, 1978,

his Table 3). Discussions with H. C. Helgeson subsequently led to calculations of a volumetric fluid-rock ratio, $(F/R)_V$, more rigorously based on measurements of reaction progress, ξ (Ferry, 1980). Using CO_2 as the tracer component,

$$(F/R)_V = \frac{V_f \xi(\nu_{CO_2} - X^{eq}\Sigma\nu_j)}{X^{eq} - X^o}, \quad (1)$$

where V_f is molar volume of the fluid; X° and X^{eq} are X_{CO_2} of the input fluid and of pore fluid at the end of fluid-rock reaction, respectively; ν is the stoichiometric coefficient of the subscripted volatile component in the mineral-fluid reaction, and the sum is over all j volatile components in the reaction, including CO_2. Volumetric fluid-rock ratios greater than likely porosity of rocks during metamorphism require infiltration of rocks by fluid as decarbonation reactions proceeded. The many values of fluid-rock ratio $\geq$0.1 reported by Ferry (1980), including values for samples from the Waterville limestone, indicated that infiltration occurred in carbonate rocks throughout the area in Fig. 1. Values of $\delta^{18}O$ of ankerite and calcite from location 7 that are 3 – 7‰ less than the range for unaltered Silurian marine carbonates are consistent with, but do not require, infiltration of the Waterville limestone with low-$\delta^{18}O$ fluids during metamorphism (Rumble et al., 1991).

Infiltration of carbonate rocks by aqueous fluid during metamorphism is more than a curiosity. When the aqueous fluid infiltrates a carbonate rock, p_{CO_2} is reduced, inducing mineral decarbonation reactions that then proceed until the mixture of infiltrating fluid and CO_2 liberated by the reactions is in equilibrium with mineral reactants and products. Thus, to the extent that mineral reactions are the essence of metamorphism from a petrologic standpoint, fluid infiltration drives metamorphism. Doug Rumble coined the term “infiltration-driven

metamorphism" to emphasize the essential link between reactive fluid flow and metamorphism. Large fluid-rock ratios have been documented also for pelitic schists and sulfidic schists of the Waterville Formation (Ferry, 1981, 1984) and for pelites, marls, psammites, and mafic and felsic metavolcanic rocks elsewhere (Ferry, 1988). Infiltration-driven metamorphism turned out to be a globally widespread phenomenon (Ague, 2003).

Most fluids trapped as inclusions in quartz from samples of the Waterville limestone and other portions of the Waterville Formation are not the H_2O-rich CO_2-H_2O fluids predicted by a process of infiltration of rock by aqueous fluid (Sisson and Hollister, 1990; Olsen and Ferry, 1995). Fluid inclusions from location 7 contain N_2 and N_2-CO_2 fluids and, based on textural relations, likely formed after the peak of metamorphism (Sisson and Hollister, 1990). Most texturally early fluid inclusions from location 5 and a location south of the area of Fig. 1 are CO_2-rich with and without some CH_4 and N_2 and with little or no H_2O. Sisson and Hollister (1990) and Olsen and Ferry (1995) interpreted the CO_2-rich fluids as possible prograde fluids. A small population of texturally primary aqueous fluids from a location south of Fig. 1 with low to moderate salinity (<7 wt% NaCl equivalent) and $X_{CO_2} < 0.05$, were identified as the kinds of H_2O-rich H_2O-CO_2 fluids expected from the petrologic evidence for infiltration-driven metamorphism (Olsen and Ferry, 1995).

Metamorphic hydrology

Even more amazingly, Bowen (1940, p. 263) predicted that channelways for metamorphic fluid flow in contact aureoles might be identified by "localized occurrences of high-grade minerals" produced by decarbonation reactions. This suggestion was first systematically pursued in the Waterville limestone (Ferry, 1987). A fundamental petrologic observation of the Waterville limestone is large, layer-by-layer differences in the progress of

mineral decarbonation reactions, even between layers no more than 1 cm thick in the same thin section, not only at locations 5 and 7 (Figs. 2a,b) but also at locations 160, 1200, and 3 (Fig. 1). Variations in reaction progress translate into calculated fluid-rock ratios that correspondingly vary across layering (cf., Equation 1). On the other hand, there are no significant variations in reaction progress, and hence fluid-rock ratio, over distances of up to ~10 m along the same layer. These results led to the conclusion that fluid flow during metamorphism was channeled along certain more permeable layers (metamorphic aquifers), some less than a cm wide. It is now recognized, however, that when mineral reactants and products are solid solutions (as they are in the Waterville limestone) cm-scale layer-to-layer differences in calculated fluid rock ratio contain no unambiguous information about the spatial distribution fluid flow during metamorphism (because of the effects of cross-layer CO_2-H_2O interdiffusion). Furthermore, even when mineral reactants and products have fixed compositions, fluid-rock ratios do not provide meaningful information about the amount of fluid that has flowed through a rock.

Transport theory: one-dimensional models

Fluid-rock ratios for a hand specimen of rock (Equation 1) accurately describe fluid-rock interaction only if minerals react with trapped, stagnant pore fluid. The fluid-rock ratio then corresponds to the porosity of the rock at the time of reaction. In this context, fluid-rock ratios >1, as are commonly reported, make no sense – the material would be a slurry rather than a rock. Applied to a flow system, a fluid-rock ratio calculation assumes the physically impossible circumstance of reactive fluid generated in one place (e.g., pure H_2O) and flowing to a site of mineral reaction at elevated *T* without reacting with any other rocks along the flow path. Proper evaluation of amounts of fluid flow from petrologic data require (a) a conceptual model of the flow system from the inlet where reactive fluid is introduced to the site of reaction downstream

where a mineral assemblage is produced that a petrologist later collects, (b) an analytical treatment of coupled flow and reaction different from the equation for a fluid-rock ratio, and (c) choice of a tracer component that couples the amount of fluid flow to measured changes in rock chemistry caused by fluid-rock reaction.

The analytical description of coupled fluid flow and chemical reaction in porous media is the advection-diffusion equation (also known as the mass continuity equation), a statement of mass balance, closely analogous to the heat equation, and long known to physical chemists and chemical engineers (e.g., De Groot and Mazur, 1962, who present the equation without derivation as self-evident). Amounts of fluid flow computed from the advection-diffusion equation are expressed as fluxes or time-integrated fluxes, the latter with units of amount of fluid per unit area perpendicular to the flow direction (e.g., cm^3 fluid/cm^2 rock, mol/cm^2, g/cm^2). Unlike fluid-rock ratios, quantities with these units are meaningful to hydrogeologists in developing hydrodynamic models of geological flow systems. The advection-diffusion equation in general form was broadly introduced to petrologists by Bickle and McKenzie (1987). Soon afterwards, Baumgartner et al. (1988) adapted the equation to decarbonation reactions driven by flow of aqueous fluid using CO_2 as the tracer component, and Baumgartner and Ferry (1991) applied it to the specific case of regional metamorphism of carbonate rocks in the area of Fig. 1. Assuming as a simplification that mineral reactants and products have fixed compositions, Baumgartner and Ferry (1991) were unable to reproduce the widespread spatial distribution of mineral reactants and products of decarbonation reactions unless flow was nearly horizontal with inlet to the flow system somewhere north of the chlorite zone and flow in the direction of increasing metamorphic grade (and *T*) from northeast to southwest in Fig. 1. Reevaluation of the petrologic data for infiltration-driven metamorphism in the area of Fig. 1 in terms of the

advection-diffusion equation rather than the fluid-rock ratio concept suggested that very large quantities of fluid were involved with time-integrated fluid fluxes in the Waterville limestone up to ~10^6 cm^3 fluid/cm^2 rock and similar values in the rest of the Waterville Formation and in the adjacent Vassalboro Formation (Ferry, 1994). Large layer-to-layer differences in calculated time-integrated fluid flux, such as at locations 5 and 160 in the Waterville limestone, were interpreted in terms of highly channeled fluid flow during regional metamorphism.

Two important problems soon emerged with the concept of horizontal, channeled fluid flow in the direction of increasing temperature during regional metamorphism. First, simple hydrodynamic models consistently predicted that regional metamorphic fluid flow should primarily be vertical, directed upwards in the direction of decreasing temperature (Hanson, 1992, 1997). Second, the interpretation that layer-to-layer differences in calculated time-integrated flux actually correspond to layer-to-layer differences in the amounts of fluid flowing through rocks during metamorphism implicitly assumes that layers in the same outcrop were chemically isolated from each other. This assumption, however, was inconsistent with evidence for significant cross-layer mass transport of CO_2 and H_2O during metamorphism both by flow and diffusion (reviewed in the following section). More such evidence soon followed, specifically, for the Waterville limestone.

Cross-layer volatile transport

Hewitt (1973) observed mineral assemblages in metamorphosed marl layers from the Wepawaug Schist that record lower X_{CO_2} at their contact with schists than in their interiors. Similarly, Rye et al. (1976) observed gradients in the oxygen isotope composition of marble layers from Naxos with lower values at their margins in contact with schists and higher values in their interiors. In both cases, the gradients in X_{CO_2} and $\delta^{18}O$ imply cross-layer volatile exchange

between carbonates and schists either by fluid flow, diffusion, or both. In a pioneering study, Bickle and Baker (1990) quantitatively interpreted $\delta^{18}O$ gradients across the marble layers on Naxos, using the advection-diffusion equation, to obtain estimates of time-integrated fluid flux and the characteristic distance of diffusion of volatiles across the carbonate layers [$\sqrt{(Dt)}$, where D is the effective diffusion coefficient and t is the duration of mass transport]. Both were non-zero quantities.

The approach used by Bickle and Baker (1990) in their study on Naxos was expanded to include measured profiles in carbon and strontium as well as oxygen isotopes, and applied to the contact between the Waterville limestone and adjacent schist of the normal Waterville Formation by Bickle et al. (1997). Quantitative inversion of profiles for all three isotopes proved significant cross-layer transport by diffusion during metamorphism at locations 5 and 7 (Fig. 1) with the exception of the oxygen profile at location 7. The characteristic diffusion distance for oxygen increased with increasing metamorphic grade from 1.5±2.0 m at location 7 to 6.4±0.4 m at location 5. The surprisingly large diffusion distance at location 5 can now be understood in terms of very fast CO_2-H_2O interdiffusion in fluid at conditions of regional metamorphism (Wark and Watson, 2004). Non-zero cross-layer time-integrated fluid fluxes were recorded by all isotope profiles at both locations except for the Sr profile at location 7. The cross-layer time-integrated fluid flux recorded by oxygen isotope transport at location 5, ~16.7 mol fluid/cm^2 rock, however, is not large enough to explain the measured values of progress of decarbonation reactions across the entire ~100 m width of the Waterville limestone at location 5. The result demonstrated that reactive fluid flow during metamorphism must have been primarily, but not exclusively, parallel to layering.

Transport theory: two-dimensional models

After 1997, the understanding of reactive fluid flow during metamorphism of the Waterville limestone and elsewhere had shifted from strictly layer-parallel flow in chemically isolated layers to primarily layer-parallel flow with small but significant volatile transport across layering by diffusion and/or flow. Accordingly, two-dimensional transport models were developed with provision for mass transport parallel to and perpendicular to layering. Evans and Bickle (1999) demonstrated that measured progress of decarbonation reactions in metamorphosed marls from the Waits River Formation, Vermont, could be explained by much smaller time-integrated fluid fluxes than those required by purely layer-parallel flow if a small component of flow occurred across layering. When marls are interbedded with schists on a scale of meters, as in the Waits River Formation and Wepawaug Schist, measured reaction progress can be explained by little or no flow in the carbonate layers (Ague and Rye, 1999; Ague, 2000). According to their models, reactive H_2O-rich fluids flow mostly or exclusively in the schist layers, and decarbonation of interbedded marls is driven by H_2O infiltration with H_2O-CO_2 interdiffusion between marl and adjacent schist as the mechanism of infiltration. The H_2O-rich fluid could be derived from dehydration reactions in the schists and/or from crystallization of synmetamorphic granitic rocks. The models of Ague and Rye (1999) and Ague (2000) predict very small differences in $X_{CO_2} \leq \sim 0.01$ within and between marl layers. The prediction, consistent with the characteristic diffusion distance for oxygen estimated by Bickle et al. (1997) for location 5 of the Waterville Formation, was subsequently verified by phase equilibrium calculations for regionally metamorphosed marls from the Wepawaug Schist (Ague, 2002).

Given the characteristic diffusion distance for H_2O-CO_2 interdiffusion of ~6 m estimated by Bickle et al. (1997), the large layer-by-layer differences in progress of decarbonation

reactions at location 5 of the Waterville limestone (Fig. 2a) demanded an explanation other than channeled flow in chemically isolated layers at a scale of centimeters. Bickle et al. (1997) recognized that time-integrated fluid flux, calculated assuming chemically isolated layers, was linearly correlated both with the inferred initial Fe/(Fe+Mg) of biotite and with the relative proportion of micaceous and carbonate minerals in individual layers. Similarly, Evans and Bickle (2005) demonstrated that layer-by-layer variations in reaction progress could be explained by layer-by-layer variations in bulk rock composition rather than by layer-by-layer variations in time-integrated fluid flux.

Penniston-Dorland and Ferry (2006) explained these observations with a quantitative model for mineral reactions involved in the formation of biotite in both the Waterville limestone and Waits River Formation. Based on the average of measured mineral compositions in the 24 samples from location 5 (Table 1A) and the assumption that fluid is a CO_2-H_2O-NaCl-$CaCl_2$ solution, the mineral-fluid system in which the biotite-forming reaction occurred contains 11 system components and 18 phase components (Ferry et al., 2013). It follows from the phase rule, therefore, that mineral-fluid reaction can be rigorously described by 18 – 11 = 7 linearly independent reactions among the phase components (Thompson, 1982). Four of these are the linearly-independent Fe-Mg exchange reactions among ankerite, calcite, biotite, muscovite, and chlorite. The other three reactions are net-transfer reactions that govern changes in the amounts of minerals present (Table 1B). Using measured modes and mineral compositions of 24 samples from location 5 and measured Fe-Mg exchange coefficients in Table 1C, initial modes and mineral compositions were reconstructed for each sample prior to initiation of reactions 1-3. Motivated by the modeling and field studies by Bickle et al. (1997), Ague and Rye (1999), and Ague (2000, 2002), mineral reactions in the 24 samples were simulated with the constraint that

X_{CO_2} was the same in all samples at each instant during reaction. At the point when the measured progress of biotite-forming reaction 1 (ξ_1) in any one sample was attained, the simulation reproduced the measured value of ξ_1 in all other 23 samples. The match between measured and calculated values of ξ_1 is not an independent prediction by the model but rather is required by the assumption that X_{CO_2} in the calculations is the same in all layers at each instant during reaction (Penniston-Dorland and Ferry, 2006). The observed layer-to-layer variations of ξ_1 at location 5 are better explained by layer-by-layer variations in initial modes and mineral compositions prior to reaction than by channeled flow in chemically isolated layers. The most important controls on reaction progress are the amount and compositions of ankerite and plagioclase in a layer at the start of reaction and the extent of Ca-Na exchange during reaction 1 between a layer and either its neighbors, the infiltrating fluid, or both.

The quantitative model for mineral reaction in the Waterville limestone was integrated with a two-dimensional model for fluid transport by Ferry et al. (2013). The model involved the same 24 layers considered by Penniston-Dorland and Ferry (2006). Mass transport by fluid flow was explicitly considered parallel to layers; volatile transport by diffusion perpendicular to layering was implicitly considered by setting X_{CO_2} the same in each layer at each instant during flow and reaction (but with X_{CO_2} in all layers evolving with time as prescribed by the model). Different directions of fluid flow were considered in different models: both horizontal in the direction of increasing T and vertical, directed upwards in the direction of decreasing P and T. By considering solid solution in mineral reactants and products and homogenization of X_{CO_2} in multiple samples by diffusion across layers, the transport model not just reproduced the measured value of ξ_1 in all 24 layers at the spatial point in the model corresponding to location 5, as required by the calculations, but further independently predicted a spatial distribution of

reactants and products of reaction 1 over a horizontal distance of several km. These matches were attained for both geometries of fluid flow and for modest values of time-integrated fluid flux of 1000 – 2000 mol fluid/cm^2 rock. Results for vertical, upward flow were consistent with the amounts and geometry of flow predicted by hydrodynamic models of regional metamorphism (Hanson 1992, 1997; Lyubetskaya and Ague, 2009); neither horizontal flow in the direction of increasing *T* nor large values of time-integrated fluid flux were required. Two other implications of the transport model were unexpected. First, with appropriate choice of the X_{CO_2} of input fluid, the model reproduced the observed spatial distribution of ξ_1 at outcrop and km scales after the flow system reached steady state. Thus, observed spatial distributions of ξ_1, in fact, can be attained for the wide range of time-integrated fluid flux ≥1000 – 2000 mol/cm^2. Second, because layer-by-layer variations in ξ_1 at the outcrop scale can be explained just by variations in initial amounts and compositions of minerals prior to reaction, spatial distributions of ξ_1 at the scale of layering contain no unambiguous information about the spatial pattern of fluid flow. Flow may have been perfectly uniform and pervasive, focused in a single fracture, or anything in-between. When mineral reactants and products are fixed in composition, however, as envisioned by Bowen (1940), spatial variations in progress of decarbonation reactions can directly image channels of focused fluid flow through metamorphic rocks.

NEW DEVELOPMENTS IN THE WATERVILLE LIMESTONE

Successful models of fluid flow and fluid-rock interaction during regional metamorphism of the Waterville limestone must quantitatively consider or reproduce the following petrologic observations: (1) layer-to-layer differences in ξ_1 at location 5 and specifically the measured values of ξ_1 in the 24 samples in Fig. 2a and Table 2; (2) small layer-to-layer differences in X_{CO_2}

at location 5 that are recorded by mineral-fluid equilibria (Ferry, 1979; Penniston-Dorland and Ferry, 2006); (3) values of ξ_1 at location 7 that are much smaller than those in samples from location 5 (Fig. 2b); (4) the occurrence of reactants and products of reaction 1 in some layers for 12.8 km between locations 5 and 7 with the absence of biotite from carbonate rocks anywhere in the Waterville Formation NE of location 7 and completion of the biotite-forming reaction SW of location 5; and (5) the occurrence of at least some samples that contain mineral reactants of reaction 1 but not biotite at locations 5, 7, and 160, Fig. 1. For comparison, models of Ferry et al. (2013) only reproduce measured values of ξ_1 in all 24 layers from location 5 and completion of the biotite-forming reaction in the Waterville Formation SW of location 5.

Geological framework of new fluid flow models

The geological framework of the new models is illustrated in Fig. 3. Lithologic layering is considered vertical. The model domain consists of 24 layers that correspond to the 24 samples from location 5 (Fig. 2a, Table 2), and they initially contain the assemblage muscovite-ankerite-quartz-calcite-plagioclase-rutile-graphite. Initial modes and mineral compositions, however, are variable as determined by present modal and mineral composition data for each layer. Spatial coordinate *x* is horizontal, parallel to layering, and increases in the direction of increasing grade of metamorphism (NE to SW in Fig. 1). Spatial coordinate *z* is vertical, increasing upwards. The origin of the coordinate system corresponds to location 5 in Fig. 1; *P*-*T* conditions at the origin are taken as 3500 bars and 450 °C (Ferry et al., 2013). The *P* and *T* gradients are assumed to be 0 and 5 °/km along the horizontal coordinate and –270 bars/km and –30 °/km along the vertical coordinate, respectively. The models consider flow in the direction of increasing *x* and *z*. Partial homogenization of fluid composition occurs by CO_2-H_2O interdiffusion perpendicular to layering. The models ignore diffusion parallel to the direction of flow and assume that flow

perpendicular to layering is negligible compared to layer-parallel flow (Bickle et al. 1997). Pressure and temperature are assumed constant at all times at each spatial point during mineral-fluid reaction. The assumption implies that the time scale of infiltration-driven reaction during regional metamorphism is short compared to the time scale on which *P* and *T* change, an assumption for which there is emerging evidence (Skelton, 2011; Zhao and Skelton, 2013).

Mineral reaction model

The model for mineral reaction in the Waterville limestone at grades of metamorphism between those at locations 5 and 7, Fig. 1, is almost identical to that of Ferry et al. (2013). Changes in modes and mineral compositions during reactive fluid flow are controlled by the three net-transfer reactions in Table 1B. Present values of progress of the three reactions [ξ_1(pres), ξ_2(pres), ξ_3(pres)] and the initial amounts and compositions of minerals in each layer prior to flow are all calculated as in Ferry et al. (2013). Selected input parameters are listed in Table 2, especially including ones that differ from those used by Ferry et al. (2013). To reproduce small differences in X_{CO_2} among layers, the present X_{an} of plagioclase is taken as the average value for each layer, which in most cases is larger than the value used by Ferry et al. (2013). This then results in different present values of ξ_3 and initial amounts of plagioclase in the layers. Present and initial amounts and compositions of muscovite, ankerite, and calcite remain unchanged. Amounts of quartz and rutile are irrelevant to the calculations.

At any point in space and time once fluid flow and reaction begins in the models, the amount of each mineral *i* in each sample (n_i in moles/cm^3) is related to ξ_1, ξ_2, and ξ_3 by:

$$n_i = n_i(0) + (\nu_{i,1})(\xi_1) + (\nu_{i,2})(\xi_2) + (\nu_{i,3})(\xi_3), \quad (2)$$

where $n_i(0)$ is the initial amount of mineral *i* in a sample prior to reaction, and $\nu_{i,j}$ is the stoichiometric coefficient of mineral *i* in reaction *j* ($\nu_{Pl,1} = +0.530$; $\nu_{Pl,2} = -1.325$; $\nu_{Pl,3} = -1$). As in Ferry et al. (2013), ξ_2 is empirically linked to ξ_1 in each layer by $\xi_2 = 0.05\xi_1$. All analyzed samples from location 7 contain albite with $X_{an} = 0.02$, regardless whether they contain reactants and products of reaction 1 or just reactants. Five samples from location 5 that contain reactants but not products of reaction 1, however, contain more calcic plagioclase with average $X_{an} = 0.23$-0.38. These samples initially must have contained albite and thus experienced significant progress of reaction 3 while ξ_1 remained zero. Samples from location 5 with estimated initial compositions of ankerite like those of ankerite in samples from location 7 with $\xi_1 > 0$, have relatively large values of ξ_1(pres). Somewhat arbitrarily, therefore, plagioclase is taken as albite with $X_{an} = 0.02$ when reaction 1 begins in the eight layers with the highest values of ξ_1(pres) with ξ_3 linked to ξ_1 by $\xi_3 = \xi_1/[\xi_3(\text{pres})/\xi_1(\text{pres})]$. In all the other layers, ξ_3 is set to the present value (Table 2) at the time reaction 1 begins. Using mass balance of Fe or Mg and the Fe-Mg exchange coefficients in Table 1C, calculated changes in n_i from Equation 2 lead to calculated changes in mineral composition.

Mineral-fluid equilibrium

The fluid flow models assume local mineral fluid-equilibrium. Values of X_{CO_2} in each layer at each point in time and space is tracked by the equilibrium:

$$\underset{\text{muscovite}}{KAl_3Si_3O_{10}(OH)_2} + 3\ \underset{\text{ankerite}}{CaMg(CO_3)_2} + 2\ \underset{\text{quartz}}{SiO_2} =$$

$$\underset{\text{biotite}}{KMg_3AlSi_3O_{10}(OH)_2} + \underset{\text{plagioclase}}{CaAl_2Si_2O_8} + 2\ \underset{\text{calcite}}{CaCO_3} + 4\ \underset{\text{fluid}}{CO_2}. \qquad (3)$$

Using the Berman (1988, updated 1992) thermodynamic database and the Kerrick and Jacobs (1981) equation of state for CO_2-H_2O fluids, values of X_{CO_2} were fit as a function of $\ln K_s$ and x (horizontal flow models) or z (vertical flow models), where

$$K_s = [(a_{KMg_3AlSi_3O_{10}(OH)_2})(a_{CaAl_2Si_2O_8})(a_{CaCO_3})^2]/[(a_{KAl_3Si_3O_{10}(OH)_2})(a_{CaMg(CO_3)_2})^3]. \quad (4)$$

The Cl-content of fluid was assumed negligible for the purpose of calculations of X_{CO_2}. Activity-composition relations adopted for mineral solid solutions are those in Ferry et al. (2013). Table 2 lists present values of $\ln K_s$ [$\ln K_s$(pres)], calculated from Equation 4 and present mineral compositions in each of the 24 layers. Initial $\ln K_s(0)$ values (when reaction initiates) and $\ln K_s$(max) values (when reaction is complete) were calculated from estimated initial mineral compositions when reaction starts and mineral compositions when either muscovite or ankerite is consumed, respectively.

The X_{CO_2} of fluid in equilibrium with each layer when it contains measured amounts of reactants and products of reaction 1 was calculated from values of $\ln K_s$(pres) in Table 2 at *P-T* conditions recorded by mineral equilibria at location 5, 3500 bars and 450 °C (open circles, Fig. 4a). Differences in X_{CO_2} between samples that contain reactants and products of reaction 3 are 0.026 or less, comparable to differences across individual layers in the Wepawaug Schist, predicted by transport modeling (Ague, 2000), and across reaction selvages between carbonate layers and adjacent quartz veins, determined from mineral assemblages and phase equilibrium calculations (Ague, 2002). Samples from location 5, in which reaction 1 has gone to completion or in which reaction 1 did not occur, set upper or lower bounds on X_{CO_2}, respectively (black triangles, Fig. 4a). The upper and lower bounds are mostly consistent with values defined by

samples with reactants and products. Layer-by-layer variations in X_{CO_2} were introduced into the fluid flow calculations by specifying that at each point in space and time the difference in $\ln K_s$ between each layer *i* and reference layer 29c ($\Delta \ln K_s$) is the same as the difference in $\ln K_s$(pres) between layer *i* and layer 29c (Table 2). Sample 29c was chosen as the reference because it contains ankerite with the largest value of $X_{FeAnk}(0)$ (Table 2) and the smallest value of $\ln K_s(0)$, and hence is the first layer to begin reaction 1 in all flow models.

The quantitative reaction model allows for calculation of mineral compositions and hence $\ln K_s$ in each layer when reaction 1 begins and at all later times when $0 < \xi_1 \leq \xi_1(\max)$. The relationship between $\ln K_s$ and ξ_1 depends only on mass balance and is independent of the *P* and *T* of reaction; an example is illustrated specifically for layer 29c in Fig. 5. Discontinuities in the slope of the curve are the result of non-ideal mixing behavior in plagioclase solid solution. For a given choice of *P* and *T* of reaction, each value of $\ln K_s$ corresponds to a value of X_{CO_2} (right-hand vertical scale, Fig. 5). Thus, any value of $\ln K_s$ for a layer uniquely defines the value of ξ_1 and vice versa, regardless of *P* and *T*; at a given *P* and *T* any value of $\ln K_s$, ξ_1, or X_{CO_2} uniquely defines the other two variables.

Vertical flow in the direction of decreasing *P* and *T*

Model tuned to measured reaction progress at location 5. Among the models considered by Ferry et al. (2013) for vertical, upward-directed fluid flow in the direction of decreasing *P* and *T*, the preferred model was one in which the composition of the input fluid to the flow system ($X^\circ_{CO_2}$) was tuned to match measured reaction progress in all 24 layers from location 5 (Fig. 2a, Table 2) in the least restrictive way. The model value of X_{CO_2} when all 24 layers developed the measured present values of ξ_1 is 0.163. If $X^\circ_{CO_2} > 0.163$, model ξ_1 is less

than measured ξ_1 in every layer for all values of time-integrated fluid flux (cf. Fig. 5; the input fluid is insufficiently reactive to drive ξ_1 to values as high as those measured). For values of $X°_{CO_2} < 0.163$, model and measured ξ_1 match only for a single value of time-integrated fluid flux (the input fluid is sufficiently reactive that, with continued flow, ξ_1 eventually is driven to values greater than those measured). For values of $X°_{CO_2} = 0.163$, however, the flow system reaches a steady state in which not only do model and measured values of ξ_1 match, but do so over a wide range of time-integrated fluid flux equal to and greater than a threshold value, ~2000 mol/cm^2 (the input fluid is just reactive enough to drive ξ_1 in all layers to measured values but not to greater values).

In the new flow model in which there are differences in X_{CO_2} among the 24 layers, a corresponding quasi-steady state is attained that reproduces measured ξ_1 in reference layer 29c with reaction 1 at 3500 bars and 450 °C, when $X°_{CO_2} = 0.159$ (Fig. 5). [The value of $X°_{CO_2}$ differs from 0.163 because calculations in this study are based on slightly different values of X_{an}(pres) than those in Ferry et al. (2013). It is a quasi-steady state because gradients in X_{CO_2} among the 24 layers are retained that in a true steady-state model would be erased by diffusion.] The value of $X_{CO_2} = 0.159$ corresponds to $\ln K_s = -1.298$ (Fig. 5). Using the values of $\Delta \ln K_s$ (Table 2), the values of $\ln K_s$ and model ξ_1 in all other layers are obtained (from diagrams analogous to Fig. 5 for each layer). Model values of ξ_1 match measured values in Fig. 2a and Table 2, as is required by the calculations.

For a value of $X°_{CO_2} = 0.159$, ξ_1 in all layers are independently predicted along any traverse through the model domain. At each spatial point along the traverse, P and T are known from the specified P and T at location 5 and the gradients in P and T (Fig. 3). The value of ξ_1 for

each of the 24 layers at that spatial point is then obtained from curves like the one for layer 29c in Fig. 5 at $X°_{CO_2}$ = 0.159 (but at the different *P*-*T* conditions and corrected for $\Delta \ln K_s$). The predicted spatial distributions of ξ_1 for five layers along a vertical traverse through location 5 are illustrated in Fig. 6a. The five layers were chosen as representative of the range in spatial locations at which reaction 1 begins and goes to completion. In the direction of increasing *T*, reference layer 29c is the first layer to begin reaction and layer 52 is that last to begin and complete reaction. Layers 8c and 72b exhibit intermediate behavior. Layer 29b is adjacent to layer 29c; the pair illustrates that the predicted spatial distribution of ξ_1 can be very different even between adjacent layers, controlled by differences in the initial amounts and compositions of minerals (Table 2). Figure 6b illustrates the predicted distribution of ξ_1 perpendicular to flow along a horizontal traverse parallel to the *x* coordinate through location 5 at the present level of exposure. For clarity, results are shown only for layers 29c and 52; curves for all other layers go from $\xi_1 = 0$ to $\xi_1 = \xi_1(\text{max})$ at intermediate values of *x* between –2.19 km and 0.43 km.

The flow model tuned to measured reaction progress at location 5 includes layer-to-layer differences in X_{CO_2} and reproduces measured values of ξ_1 in all 24 layers at the spatial point that corresponds to location 5. The predicted distribution of coexisting reactants and products, however, extends only 2.6 km along the horizontal traverse (Fig. 6b), far short of the observed 12.8 km distance between locations 5 and 7. Furthermore, the model fails to predict values of $\xi_1 > 0$ in even some of the 24 layers at the spatial point in the model that corresponds to location 7.

Model tuned to measured reaction progress at location 7. A quasi-steady-state model for vertical, upward-directed fluid flow in the direction of decreasing *P* and *T* was similarly developed by tuning $X°_{CO_2}$ so that model and measured ξ_1 match at location 7 as best as possible and in the least restrictive manner. For eight analyzed samples from location 7, ξ_1 = 0.023-0.103

mol/cm^3 in four, and $\xi_1 = 0$ in the other four (Fig. 2b). The outcrop average ξ_1 is 0.030 mol/cm^3. The eight samples from location 7 have different bulk compositions, and hence different initial amounts and compositions of minerals prior to reaction, than any of the 24 samples from location 5. Accordingly, any flow model based on the samples from location 5 cannot exactly reproduce the measured values of ξ_1 in all eight samples from location 7 for any combination of $X°_{CO_2}$ and time-integrated fluid flux. The value of $X°_{CO_2}$ therefore was tuned to reproduce the outcrop average value of $\xi_1 = 0.030$ mol/cm^3 at location 7. The average measured $\xi_1 = 0.030$ mol/cm^3, with reaction 1 at 3500 bars and 386 °C (model *P*-*T* conditions at location 7, Fig. 3), is reproduced when the input fluid has $X°_{CO_2} = 0.0155$ (Fig. 2c). When $X°_{CO_2} = 0.0155$, the model qualitatively predicts that the 24 layers either are unreacted or have relatively small values of ξ_1 (Fig. 2c), similar to what is observed at location 7 (Fig. 2b). Taking, as before, layer 29c as the reference layer that equilibrates with the input fluid and the values of $\Delta \ln K_s$ in Table 2, corresponding values of X_{CO_2} (for layers with reactants and products) or lower bounds on X_{CO_2} (for unreacted layers) can be computed (Fig. 4b). Although calculated values of X_{CO_2} at location 7 (Fig. 4b) are ~10 times smaller than at location 5 (Fig. 4a), ratios are similar because equal differences in $\ln K_s$ approximately correspond to equal ratios in X_{CO_2}.

With $X°_{CO_2} = 0.0155$, predicted spatial distributions of ξ_1 were calculated for the same five representative layers along a vertical traverse through location 7 and for layers 29c and 52 along a horizontal traverse parallel to the *x* coordinate through location 7 (Fig. 7). For clarity, spatial distributions of ξ_1 are shown only for two layers in Fig. 7b; curves for all other layers go from $\xi_1 = 0$ to $\xi_1 = \xi_1(\text{max})$ at intermediate values of *x* between –12.90 km and –11.17 km. The flow model tuned to measured reaction progress at location 7 includes layer-to-layer differences

in X_{CO_2} and reproduces the average measured value of ξ_1 at the spatial point that corresponds to location 7 (as is required by the calculations). The predicted distribution of coexisting reactants and products, however, extends only 1.7 km along the horizontal traverse (Fig. 7b), far short of the observed 12.8 km distance between locations 5 and 7. Furthermore, contrary to measured values (Fig. 2a, Table 2), the model fails to predict values of $\xi_1 = 0$, or even $\xi_1 < \xi_1(\max)$, in any of the 24 layers at the spatial point in the model that corresponds to location 5.

Model with spatially variable $X°_{CO_2}$. Models for vertical fluid flow in the direction of decreasing *P* and *T* with a single value of $X°_{CO_2}$ can either reproduce the measured values of ξ_1 at location 5 or the average of measured values of ξ_1 at location 7 but not both. A third model therefore was developed with a spatial variation in $X°_{CO_2}$ in the horizontal dimension parallel to the *x* coordinate. To reproduce measured ξ_1 at location 5 and average ξ_1 at location 7, $X°_{CO_2}$ was set to 0.159 at $x = 0$ (corresponding to location 5 in the model, Fig. 3) and to 0.0155 at $x = -12.8$ km (corresponding to location 7). Additionally, based on a calculation of X_{CO_2} from Equilibrium 3 at 3500 bars and 430 °C for a sample from location 160 that contains reactants and products of reaction 1 (Table 1), $X°_{CO_2}$ was set to 0.0758 at $x = -4.0$ km (corresponding to location 160). A quadratic fit of *x* to the three data defines a nearly linear relation between $\ln X°_{CO_2}$ and *x* (Fig. 8; data are the small circles). The quadratic $\ln X°_{CO_2}$-*x* relation leads to the predicted completion of reaction 1 in all 24 layers ~ 1km SW of the location 5 ($x = 1.2$ km), consistent with field observations. The quadratic $\ln X°_{CO_2}$-*x* relation, contrary to field observations, predicts coexisting reactants and products over a distance of 5-10 km NE of location 7 ($x = -18$ to -23 km). To reproduce the absence of biotite from all carbonates rocks from the Waterville Formation NE of

location 7, $X°_{CO_2}$was set at a constant value of 0.0155 for all values of $x \leq -12.8$ km (dashed and solid curves, Fig. 8).

With $X°_{CO_2}$ defined by the dashed curve in Fig. 8, predicted spatial distributions of ξ_1 were calculated for the same five representative layers along a horizontal traverse through locations 7 and 5 parallel to the *x* coordinate at the present level of exposure (Fig. 9). Predicted spatial distributions of ξ_1 in the five samples along vertical traverses through locations 5 and 7 are identical to those in Figs. 6a and 7a, respectively (because $X°_{CO_2}$ is the same). The flow model with spatially variable $X°_{CO_2}$ overcomes the shortcomings of all previous flow models for regional metamorphism of the Waterville limestone: (1) it includes small layer-to-layer differences in X_{CO_2} at all spatial points in the model, (2) it reproduces the measured values of ξ_1 in all 24 layers at the spatial point that corresponds to location 5 and the average measured value of ξ_1 at the spatial point that corresponds to location 7, (3) it predicts a distribution of coexisting reactants and products in some layers along a horizontal traverse parallel at the present level of exposure extending 14.2 km and passing through the spatial points that correspond to locations 5 and 7 (Fig. 9), (4) it predicts $\xi_1 = 0$ in all 24 layers a short horizontal distance (0.1 km) NE of location 7 and $\xi_1 = \xi_1(\text{max})$ in all 24 layers a short horizontal distance (1.2 km) SW of location 5 (Fig. 9), (5) it predicts at least some layers that contain all mineral reactants of reaction 1 remain unreacted ($\xi_1 = 0$) over the entire distance between locations 5 and 7 (e.g., layer 52, Fig. 9), and (6) it predicts that different layers start and complete reaction 1 at different spatial points along the horizontal traverse between locations 5 and 7 (Fig. 9). The model for spatially variable $X°_{CO_2}$ thus accurately reproduces observed values of the progress of reaction 1 at spatial scales spanning more than six orders of magnitude from differences in ξ_1 between adjacent cm-thick

layers at location 5 (e.g., layers 29b and 29c, Fig. 2a) to coexisting reactants and products [$0 < \xi_1 < \xi_1(\max)$] in some layers over the distance of 12.8 km between locations 5 and 7 (e.g., layers 8c and 29c, Fig. 9).

Horizontal flow in the direction of increasing *T*

An additional goal of this study was to evaluate the possibility that horizontal, isobaric flow in the direction of increasing *T* could be disproved with petrologic data. Specifically, the time-integrated input fluid flux ($q°$) of horizontal up-*T* flow was calculated to reproduce the average value of $\xi_1 = 0.030$ mol/cm^3 at the point in the model corresponding to location 7. If that value of $q°$ predicted either much lower or much higher values of ξ_1 than the measured values in the 24 layers at the point in the model that corresponds to location 5 (Fig. 2a, Table 2), then horizontal up-*T* flow would be ruled out on petrologic as well as hydrodynamic grounds. In a layered medium in which minerals are solid solutions, the relationship between $q°$ and reaction progress in the *p* layers at any point in the flow system then is:

$$q° = \sum_{\mathrm{i}=1}^{\mathrm{p}} \left\{ VF(\mathrm{i}) \int_0^{\xi^{\mathrm{f}}(\mathrm{i})} R°(\mathrm{i}) \mathrm{d}\xi(\mathrm{i}) \right\}, \tag{5}$$

where VF(i) is the volume fraction of layer i, ξ^{f}(i) is the final value of ξ in layer i,

$$R°(\mathrm{i}) = \frac{\{\nu_{CO_2} - X^{\mathrm{eq}}(\mathrm{i})[\nu_{CO_2} + \nu_{H_2O}]\}^2}{[\partial X^{\mathrm{eq}}(\mathrm{i}) / \partial x][\nu_{CO_2} - X^{\mathrm{o}}(\nu_{CO_2} + \nu_{H_2O})]}, \tag{6}$$

ν_{CO_2} and ν_{H_2O} are the stoichiometric coefficients of CO_2 and H_2O in the reaction, X^{eq}(i) and $\partial X^{\mathrm{eq}}(\mathrm{i})/\partial x$ are the composition and gradient in composition of fluid in equilibrium with layer i at a

given value of ξ, and $X°$ is the composition of the input fluid to the flow system (Ferry et al., 2013). Variables specific to a particular layer are distinguished with "i" and all other variables are the same for all layers. Equation (6) quantitatively accounts for fluid production between the inlet to the flow system and any point where mineral-fluid reaction occurs downstream. The 24 layers are considered equal in thickness; hence $VF(\mathrm{i}) = 0.0417$ for all layers. Because $\xi_2 = 0.05\ \xi_1$, ν_{CO_2} and ν_{H_2O} are +2.837 and –0.222, respectively, for all layers (Table 1B). Values of $X^{eq}(\mathrm{i})$ and $\partial X^{eq}(\mathrm{i})/\partial x$ as a function of $\xi(\mathrm{i})$ were calculated for each layer from fits of $\ln K_s$ and X^{eq} against x at $z = 0$ in the model domain (Fig. 3). From Fig. 8, $X° = 0.0155$.

The value of $q°$ that reproduces the average value of $\xi_1 = 0.030$ mol/cm^3 at the point in the model corresponding to location 7 is 3124 mol/cm^2. For this value of $q°$, ξ_1 in all 24 layers at the point in the model corresponding to location 5 would be $\xi_1(\mathrm{max})$, greater than measured values in all but two layers (Table 2). With $X° = 0.0155$, ξ_1 reaches $\xi_1(\mathrm{max})$ in all 24 layers from location 5 at the slightly smaller value of $q° = 2798$ mol/cm^2. At the *P*-*T* conditions corresponding to location 5, however, calculated values of $q°$ are sensitive to small differences in the assumed *T* of reaction. For a $q°$ of 3124 mol/cm^2, calculated and measured values of ξ_1 match at location 5 if the *T* of reaction is 446 °C rather than 450 °C. The lower *T* of reaction can be plausibly explained in two ways. First, *T* of reaction might simply have been 4 °C less than assumed. Second, reaction at location 5 could have occurred over a range of *T* starting below and ending at 450 °C with an effective average *T* of reaction of 446 °C. Granting even a very small uncertainty in the effective *T* of reaction at location 5, the possibility that measured values of ξ_1 in the 24 layers from location 5 and the average ξ_1 of layers at location 7 could have been produced by horizontal flow in the direction of increasing *T* with $q° \approx 3100$ mol/cm^2 cannot be unequivocally ruled out.

Uncertainties

Uncertainties in results of the model calculations that reproduce observed layer-to-layer variations in ξ_1 at the scale of outcrops, that predict the spatial distribution of reactants and products of reaction 1 over distances of up to ~15 km in three dimensions, and that estimate values of time-integrated inut fluid flux ($q°$) result from uncertainties in values of some but not necessarily all of the input variables. Regardless whether fluid flow is vertical or horizontal, calculation of layer-to-layer variations in ξ_1 (Fig. 2) are fundamentally based on mass balance independent of P, T, and $X°_{CO_2}$ during mineral-fluid reaction. The calculations are structured so that target values of ξ_1 are exactly reproduced for any given set of present values of ξ_1 in the 24 layers and for any given set of average mineral compositions. Target variations in ξ_1 are also reproduced if mineral compositions differ from one layer to another (and hence also the stoichiometry of reactions 1 and 2, Table 2B) although calculations then are more involved.

Regardless whether fluid flow is vertical or horizontal, for any set of present values of ξ_1 in the 24 layers and for any set of average mineral compositions, the predicted spatial distribution of reactants and products of reaction 1 in x direction of the model domain at the present level of exposure, $z = 0$ (e.g., Fig. 9) depend on P and T only to the extent that the two variables control the values of $X°_{CO_2}$. Once P and T values consistent with observed mineral assemblages are specified along the x coordinate at $z = 0$, the choice of a single value of $X°_{CO_2}$ (horizontal flow) or a relationship between $X°_{CO_2}$ and x (vertical flow) can be found that reproduces the observed occurrence of reactants and products of reaction 1 over the 12.8 km distance between locations 7 and 5. The effects of changes in T and P oppose each other. If T in the model domain is higher than values used in this study (and/or P is lower) values of $X°_{CO_2}$ that predict coexisting reactants and products of reaction 1 between locations 7 and 5 simply are greater than those in this study. If

T in the model domain is lower (and/or *P* is higher) values of $X^{\circ}_{CO_2}$ that predict coexisting reactants and products of reaction 1 between locations 7 and 5 are lower.

Details of the predicted spatial distribution of reactants and products of reaction 1 in the vertical dimension of the model domain during vertical fluid flow (e.g., Figs. 6a, 7a) depend on *P*, *T*, and the gradients in *P* and *T* along the flow path. The effects of changes in *T* and *P* again oppose each other. If *T* along the vertical flow path is higher than values adopted in this study (and/or *P* is lower) the predicted widespread occurence of reactants and products of reaction 1 is simply shifted to shallower depths (greater values of *z*). If *T* is lower than values adopted in this study (and/or *P* is higher) the predicted widespread occurence of reactants and products of reaction 1 is shifted to greater depths (smaller values of *z*). The effect of different *T* of mineral-fluid reaction, as an example, is illustrated quantitatively by comparing Figs. 6a and 7a. If the gradient in *T* along the vertical flow path is lower than the value used in this study (and/or the gradient in *P* is higher) the predicted distance along the flow path where reactants and products of reaction 1 coexist expands. If the gradient in *T* along the vertical flow path is higher than the value used in this study (and/or the gradient in *P* is lower) the predicted distance along the flow path where reactants and products of reaction 1 coexist contracts.

For horizontal fluid flow, the most important variable controlling the calculated value of q° is *T*. The effects of ξ (within the error of measurements in Fig. 2), of mineral composition (within the measured range) and hence reaction stoichiometry, of *P*, and of the gradient in *T* are secondary. Fluid salinity is not a significant factor unless the input fluid was a highly saline brine (Ferry and Gottschalk, 2009), an unlikely circumstance considering fluid inclusion data for carbonate rocks in the area of Fig. 1 and nearby (Sisson and Hollister, 1990; Olsen and Ferry, 1995). Because of the strong curvature of mineral-fluid equilibria on T-X_{CO_2} diagrams (e.g., Fig.

11), T primarily controls $q°$ by determining $\partial X^{eq}/\partial x$ in Equation (6) [$\partial X^{eq}/\partial x = (\partial X^{eq}/\partial T)(\partial T/\partial x)$, where $\partial X^{eq}/\partial T$ is the inverse of the slope of the equilibrium curve on a T-X_{CO_2} diagram and $\partial T/\partial x$ is the horizontal gradient in T along the flow path]. As an example, the $q°$ that reproduces observed values of ξ_1 in the 24 layers at location 5 with horizontal flow in the direction of increasing T and $X°_{CO_2} = 0.0155$, is 2213 mol fluid/cm^2 rock if the T of mineral-fluid reaction at location 5 is taken as 450 °C and 4631 mol/cm^2 if T is just 10° lower, 440 °C. For vertical fluid flow, the most important variable controlling the calculated value of $q°$ is the assumed location of the inlet to the flow system at depth. The depth to inlet in this study was somewhat arbitrarily taken as 1 km below the present surface of exposure as a compromise between plausible limits of 200 m and 5 km below the surface. Because the calculated value of $q°$ for vertical fluid flow scales approximately with depth to inlet, the importance of other variables in the calculation, including salinity, is secondary. Thus, for both horizontal fluid flow in the direction of increasing T and for vertical flow in the direction of decreasing T, uncertainties in calculated $q°$ may be as large as a factor of ~5.

Plagioclase revisited

Research on the Waterville Formation was initially motivated by the possibility of using compositions of plagioclase in the metamorphosed carbonate rocks to define one or more miscibility gaps in Ca-rich plagioclase solid solutions, as Crawford (1966) did with the peristerite gap. The goal was never realized because individual samples never contain coexisting plagioclase pairs with different but uniform composition. Forty years of research in the Waterville limestone, nevertheless, has revealed new insights into controls on plagioclase composition during regional metamorphism.

Assuming all rocks in the Waterville limestone initially contained albite ($X_{an} = 0.02$), as they do at location 7 and at lower grades, with two exceptions, the present average X_{an} of plagioclase in the 24 layers from location 5 is greater than can be explained by the combined progress of reactions 1 and 2 alone during metamorphism. This discrepancy is formally demonstrated by the positive values of ξ_3(pres) for all but two layers in Table 2. Only in layer 82A is $\xi_3 < 0$; $\xi_3 = 0$ within error of measurement in layer 29c. Measured values of ξ_3(pres) in Table 2 require that all rocks other than layer 29c exchanged Na and Ca both with each other and with the infiltrating fluid during metamorphism. The predominance of layers that record $\xi_3 > 0$ further requires that Ca-Na exchange between rock and fluid at location 5 resulted in a net loss of Na from and gain of Ca in the outcrop as a whole. Similar losses of Na and K during regional metamorphism of marls have been documented for the adjacent Vassalboro Formation in the area of Fig. 1 (Ferry, 1983) and inferred for the Waits River Formation, Vermont (Ferry, 1992; Evans and Bickle, 1999).

A record of the effects of Ca-Na exchange during metamorphism among the 24 layers from location 5 of the Waterville limestone is observed in the quantitative model for mineral reaction. Figure 10 illustrates the change in X_{an} in reference layer 29c and selected other layers predicted by the model as a function of ξ_1. Curves in Fig. 10 are based strictly on mass balance and are independent of P, T, and X_{CO_2} during reaction. The curve for layer 29c (solid black) exhibits two discontinuities in slope (imperceptible at the scale of Fig. 10), one at $X_{an} = 0.22$ ($\xi_1 = 0.340$ mol/cm^3) where plagioclase changes from coexisting albite ($X_{an} = 0.02$) and oligoclase ($X_{an} = 0.22$) to a single plagioclase with $X_{an} > 0.22$, and the other at $X_{an} = 0.421$ ($\xi_1 = 0.956$) where a_{an} becomes independent of X_{an} (see Penniston-Dorland and Ferry, 2006, for further details). Analogous curves were calculated for the other 17 layers from location 5 in which

reaction 1 proceeded. Curves for six representative samples were plotted on Fig. 10 by correlating values of ξ_1 in each layer with a corresponding value of ξ_1 in layer 29c as follows. A given value of ξ_1 in a sample corresponds to a unique value of $\ln K_s$ (Fig. 5). Applying the values of $\Delta \ln K_s$ in Table 2, the corresponding value of $\ln K_s$ and hence ξ_1 in layer 29c is calculated. Even when a_{an} is constant in a layer, $\ln K_s$ changes with ξ_1 because of the effects of Fe-Mg partitioning among biotite, chlorite, muscovite, ankerite, and calcite. The curves in Fig. 10 effectively show the model time evolution of plagioclase composition of all seven samples, using progress of reaction 1 in layer 29c as a proxy for time. Curves for the layers other than 29c exhibit discontinuities in slope where they intersect the thin solid vertical and horizontal lines in Fig. 10.

The curves diverge greatly in the lower left sector ($X_{an} < 0.22$, $\xi_1(29c) < 0.340$ mol/cm^3) and the upper right sector ($X_{an} > 0.421$, $\xi_1(29c) > 0.956$ mol/cm^3) of Fig. 10. The divergence is because a_{an} is fixed in all layers in these sectors and Ca-Na exchange among samples is therefore impossible. In contrast, curves in the other parts of the diagram cluster in one of two groups. Fourteen of 18 layers in which $\xi_1 > 0$ at location 5 lie in a group near the curves for samples 3, 29c, 57, 72b, and 87; the other four lie in a cluster near curves for 17b and 89b. The clusters include both layers that contain albite ($X_{an} = 0.02$) at the start of reaction 1 (3, 29c, 87, 89b) and layers that contain a more calcic plagioclase at the start of reaction 1 (17b, 57, 72b). The clustering is most simply explained by efficient Ca-Na exchange among layers in each group that nearly homogenized plagioclase composition as reaction 1 proceeded. The clustering of curves is limited to the period of mineral-fluid reaction when layers contained plagioclase with $0.22 < X_{an} < 0.421$ because, within the context of the model, that is the only range in composition in which a_{an} can change and gradients in plagioclase composition can drive interdiffusion of Ca and Na. It

is not understood, however, why the samples cluster into two groups rather than only one or more than two.

DISCUSSION

Spatial distribution of reaction progress and fluid composition at the outcrop scale

If minerals are fixed in composition, outcrop-scale variations in progress of infiltration-driven decarbonation reactions can directly image the flow paths of reactive fluids, as Bowen (1940) recognized. This study confirms, however, that if mineral reactants and products are solid solutions and if fluid composition is even imperfectly homogenized across layers by volatile diffusion at a scale larger than layer thickness (Fig. 4), layer-by-layer differences in reaction progress at the cm scale are be explained by differences in the initial compositions and amounts of minerals prior to reaction rather than by layer-scale variations in time-integrated fluid flux. In the case of the Waterville limestone, Bickle et al. (1997) specifically identified that initial X_{Fe} of minerals is an important compositional control and that the initial relative proportions of mica and carbonate minerals is an important modal control. This study, as well as Penniston-Dorland and Ferry (2006) and Ferry et al. (2013), demonstrates that the initial amount and composition of plagioclase and Ca-Na exchange among layers and fluid (i.e., ξ_3) are important as well. Initial amounts and compositions of muscovite and calcite are less important because they exhibit a much narrower range of solid solution. As Bickle et al. (1997) suggested, layers that exhibit elevated values of ξ_1, do so because they started reaction earlier and reacted longer than other layers during metamorphism (see also Fig. 19 of Penniston-Dorland and Ferry, 2006, and Figs. 16 and 17 of Ferry et al., 2013). This study demonstrates in more detail that high-ξ_1 layers like 8c and 29c (Fig. 9) began reaction earlier and reacted longer than low-ξ_1 layers like 29b, 52, and 72b because they initially contained ankerite with higher X_{Fe} and plagioclase with lower X_{an} prior

to initiation of reaction 1 (Table 2), and because they had different histories of Ca-Na exchange with their neighbors and coexisting fluid. Specifically, the relatively higher ξ_3 in layers like 29b, 52, and 72b (Table 2) inhibited progress of reaction 1 by raising X_{an} and a_{an} (cf., Equation 4).

Differences in X_{CO_2} recorded by equilibrium 2 among the 24 samples from location 5 (Fig. 4a) can be explained in two ways. First, if small differences in $X°_{CO_2}$ occurred over spatial distances of more than ~6 m across layering, the differences would fail to be completely homogenized during metamorphism by CO_2-H_2O interdiffusion (Bickle et al., 1997). Second, lower bounds on $X_{CO_2} > 0.159$ (Fig. 4a) could be explained by equilibration of samples with the relatively CO_2-rich fluids present when reaction initiated in layers like 29c (Fig. 5) and a later failure of some of these samples to fully reequilibrate with the evolving, progressively more H_2O-rich fluids in layers like 29c as reaction 1 proceeded further (for example, by a reduction in porosity). If true, the implication is that porosity and permeability of the 24 layers behaved differently with time during metamorphism.

Spatial distribution of reaction progress at the regional scale

If mineral reactants and products of an infiltration-driven metamorphic decarbonation reaction are fixed in composition, fluid flow in the direction of decreasing *T* produces a sharp reaction front separating completely reacted rocks upstream from completely unreacted rocks downstream. If reactants and products are solid solutions, if the flow medium is composed of multiple layers with different initial amounts and compositions of minerals prior to reaction, and if fluid composition is homogenized across layering by diffusion, fluid flow in the direction of decreasing *T*, however, can produce broad reaction fronts with coexisting reactants and products distributed for a significant distance along the flow path (Ferry et al., 2013). This study additionally demonstrates, in the specific case of reaction 1 in the Waterville limestone, that a

widespread distribution of reactants and products develops during down-*T* flow even if cross-layer homogenization of fluid composition is imperfect. Furthermore, the spatial distribution of reactants and products in the horizontal dimension parallel to the metamorphic field gradient can be much larger, ~13 km or more, as is observed in the Waterville limestone, if there is a horizontal gradient in the composition of the input fluid in the metamorphic terrain (Fig. 9).

Vertical flow in the direction of decreasing temperature or horizontal flow in the direction of increasing temperature?

There are numerous arguments why fluid flow during regional metamorphism is expected to normally have a large vertical component, directed upwards. First, hydrodynamic models of regional metamorphism predict mostly vertical, upward flow (Hanson, 1992, 1997; Lyubetskaya and Ague, 2009). Fluid flow in the direction of increasing *T* during regional metamorphism may be limited to somewhat special circumstances such as in the vicinity of large sill-shaped plutons (Ague and Lyubetskaya, 2010). Second, numerical simulations of upward fluid flow during regional metamorphism through a sequence of interlayered carbonate rock and schist reproduce the mineral assemblages and mineral reactions observed in natural examples of infiltration-driven metamorphism like the Waits River Formation and Wepawaug Schist (Rye and Ague, 1999; Ague, 2000). Third, three-dimensional inversions of the spatial distribution of the progress of carbonation and decarbonation reactions and of oxygen and carbon isotope compositions of minerals in metamorphic terrains predict upward-directed, layer-parallel flow, except in the vicinity of fold hinges (Skelton et al., 1997; Wing and Ferry, 2002). Fourth, the measured values of ξ_1 in 24 samples from location 5, the average measured value of ξ_1 in 8 samples from location 7, and the occurrence of mineral reactants and products of reaction 1 over a distance of ~13 km parallel to the metamorphic field gradient in Fig. 1 all are consistent with vertical down-*T* flow.

The gradient in input fluid composition between $X°_{CO_2} = 0.0155$ at location 7 and $X°_{CO_2} = 0.159$ at location 5, required to reproduce the ~13 km distribution of coexisting reactants and products, qualitatively makes sense in terms of vertical flow. Because the degree of decarbonation of rocks in the area of Fig. 1 increases with increasing grade of metamorphism (Ferry, 1976), upward flowing fluid would be expected to have higher $X°_{CO_2}$ in regions of higher grade metamorphism and lower $X°_{CO_2}$ in regions of lower grade metamorphism. Finally, the inferred decrease in whole-rock sodium contents in the Waterville limestone during prograde metamorphism, required by the predominantly positive values of ξ_3 in Table 2, is also consistent with down-*T* flow. Because Na/Ca of aqueous fluid is greater than Na/Ca of coexisting plagioclase (Orville, 1972), vertical fluid flow in the direction of decreasing *T* inevitably strips Na from (and adds Ca to) plagioclase in rocks along the flow path.

In spite of all these persuasive arguments, however, petrologic data fail to unambiguously disprove the possibility of isobaric, horizontal flow in the direction of increasing *T*. While it is possible only in the special case of $q° \approx 3100$ mol/cm^2, isobaric up-*T* flow can also reproduce measured values of ξ_1 in 24 samples from location 5, the average measured value of ξ_1 in eight samples from location 7, and coexisting mineral reactants and products of reaction 1 in some layers over a distance of ~13 km parallel to the metamorphic field gradient in Fig. 1.

An additional argument can be mustered in favor of horizontal up-*T* flow during regional metamorphism, at least in the Waterville limestone. Horizontal up-*T* flow readily explains the specific relation between $X°_{CO_2}$ and distance in Fig. 8 that is required to reproduce the ~13 km-long distribution of reactants and products of reaction 1 in the area of Fig. 1. The gray envelope in Fig. 11 illustrates the *T*-X_{CO_2} conditions prescribed by equilibrium between CO_2-H_2O fluid and reactants and products of reaction 1 in sample 29c. Boundaries of the envelope are defined

by $\xi_1 = 0$ and $\xi_1 = \xi_1(\text{max})$ in the sample. The T-X_{CO_2} conditions implied by the dashed curve in Fig. 8 (considering T = 450 °C at x = 0 and $\partial T/\partial x$ = 5 °/km, Fig. 3) is represented by the red curve in Fig. 11; the red curve falls entirely with the T-X_{CO_2} envelope defined by mineral-fluid equilibrium in sample 29c over the range in T between 386 °C (location 7 in the model) and 450 °C (location 5). The T-X_{CO_2}-x conditions needed to reproduce coexisting reactants and products of reaction 1 over the ~13 km distance between locations 5 and 7 therefore would be an inevitable consequence of buffering of fluid composition by reaction 1 in samples like 29c during horizontal up-T fluid flow. In contrast, in the case of vertical down-T flow, the widespread distribution of reactants and products of reaction 1 between locations 5 and 7 would represent the mineralogical adjustment of rocks in the Waterville limestone to an externally-imposed regional horizontal gradient in X_{CO_2} (Fig. 8) caused by increasing degrees of decarbonation of rocks at depth in the direction of increasing grade of metamorphism. It might seem a surprising coincidence that the externally imposed gradient in X_{CO_2} just happened to fall entirely with the range that stabilizes coexisting reactants and products of reaction 1 in samples like 29c (i.e., within the gray band of Fig. 11).

IMPLICATIONS

Forty years of research in the Waterville limestone is testimony to the value of a specific field area that continually serves as a natural laboratory both for development of new concepts and for retirement of old concepts that do not withstand closer examination. Studies of metamorphism of the Waterville limestone specifically have contributed to establishing the accepted concepts of buffering of fluid composition by metamorphic devolatilization reactions, infiltration of rocks by chemically reactive fluids, infiltration-driven metamorphism, use of the

spatial distribution of isotope compositions to constrain the geometry of metamorphic fluid flow, and outcrop-scale control of metamorphic mineral reactions by diffusion of CO_2, H_2O, and other volatile species across layering at a scale larger than layer thickness. Research on the Waterville limestone, on the other hand, initially lead to development of the concepts of the petrologic fluid-rock ratio and of horizontal fluid flow in the direction of increasing *T* during regional metamorphism that later investigations, both in the Waterville limestone and elsewhere, proved to be problematic. It is unlikely that the problems with fluid-rock ratios and horizontal up-*T* fluid flow would have been recognized and accepted as quickly if the concepts hadn't been discredited by work in the same area where they were developed.

The Waterville limestone still holds puzzles whose eventual solutions will further advance the understanding of fluids, fluid flow, and fluid-rock interaction during metamorphism. Among these include a more definite explanation of the development of coexisting reactants and products of reaction 1 over the 12.8 km distance between locations 7 and 5 and of the causes, sources, and sinks of Na metasomatism observed at the scale of location 5 and at larger spatial scales. Perhaps most importantly, however, continued studies of the Waterville limestone are a reminder that mineral devolatilization reactions are driven during metamorphism by fluid flow as well as changes in *P* and *T*, that fluid composition inevitably changes with reaction progress when mineral reactants and products are solid solutions, and that mineral and whole-rock compositions change by open system exchange of cations both among nearby layers by diffusion and between layers and flowing metamorphic fluid. All these phenomena need to be explicitly considered if interpretations of mineral assemblages and mineral compositions in hand specimens in terms of metamorphic process are to be correct.

ACKNOWLEDGMENTS

Research supported by the National Science Foundation (grant number EAR-1118713). I warmly thank Jay Ague, Lukas Baumgartner, Mike Bickle, Katy Evans, Brooks Hanson, Peter Nabelek, Doug Rumble, and Danny Rye, all of my Ph.D. students, and many others for contributing over the last 40 years to my better understanding of metamorphism. The paper was improved by the thoughtful, constructive reviews of Jay Ague, Katy Evans, and Sarah Penniston-Dorland.

REFERENCES CITED

Ague, J. J. (2000) Release of CO_2 from carbonate rocks during regional metamorphism of lithologically heterogeneous crust. Geology, 28, 1123-1126.

_____ (2002) Gradients in fluid composition across metacarbonate layers of the Wepawaug Schist, Connecticut, USA. Contributions to Mineralogy and Petrology, 143, 38-55.

_____ (2003) Fluid flow in the deep crust. In: R. L. Rudnick, Vol. Ed. The Crust. Treatise on Geochemistry Volume 3, p. 195-228. Elsevier, Amsterdam.

Ague, J. J., and Rye, D. M. (1999) Simple models of CO_2 release from metacarbonates with implications for interpretation of directions and magnitudes of fluid flow in the deep crust. Journal of Petrology, 40, 1443-1462.

Baumgartner, L. P., and Ferry, J. M. (1991) A model for coupled fluid-flow and mixed-volatile mineral reactions with applications to regional metamorphism. Contributions to Mineralogy and Petrology, 106, 273-285.

Baumgartner, L. P., Ferry, J. M., and Phillips, O. M. (1988) Infiltration driven mixed volatile reactions: A continuum mechanics approach. EOS, Transactions of the American Geophysical Union, 69, 467.

Berman, R. G. (1988) Internally-consistent thermodynamic data for minerals in the system

Na_2O-K_2O-CaO-MgO-FeO-Fe_2O_3-Al_2O_3-SiO_2-TiO_2-H_2O-CO_2. Journal of Petrology, 29, 445-522.

Bickle, M. J., and Baker, J. (1990) Advective-diffusive transport of isotopic fronts: An example from Naxos, Greece. Earth and Planetary Science Letters, 97, 78-93.

Bickle, M. J., and McKenzie, D. P. (1987) The transport of heat and matter by fluids during metamorphism. Contributions to Mineralogy and Petrology, 95, 398-392.

Bickle, M. J., Chapman, H. J., Ferry, J. M., Rumble, D., III, and Fallick, A. E. (1997) Fluid flow and diffusion in the Waterville limestone, south-central Maine: Constraints from strontium, oxygen and carbon isotope profiles. Journal of Petrology, 38, 1489-1512.

Bowen, N. L. (1940) Progressive metamorphism of siliceous limestone and dolomite. Journal of Geology, 48, 225-274.

Carmichael, D. M. (1970) Intersecting isograds in the Whetstone Lake area, Ontario. Journal of Petrology, 11, 147-181.

Chayes, F. (1956) Petrographic Modal Analysis: An Elementary Statistical Appraisal. 113 p. Wiley, New York.

Crawford, M. L. (1966) Composition of plagioclase and associated minerals in some schists from Vermont, U.S.A., and South Westland, New Zealand, with inferences about the peristerite solvus. Contributions to Mineralogy and Petrology, 13, 269-294.

De Groot, S. R. and Mazur, P. (1962) Non-equilibrium Thermodynamics, 510 p. North-Holland, New York.

Essene, E. J. (1982) Geologic thermometry and barometry. In J.M. Ferry, Ed., Characterization of Metamorphism through Mineral Equilibria, 10, p. 153-206. Reviews in Mineralogy, Mineralogical Society of America, Chantilly, Virginia.

Evans, B. W. (2007) Landmark Papers: Metamorphic Petrology. 332 p. Mineralogical Society of Great Britain & Ireland, Twickenham.

Evans, K. A., and Bickle, M. J. (1999) Determination of time-integrated metamorphic fluid fluxes from reaction progress of multivariant assemblages. Contributions to Mineralogy and Petrology, 134, 277-293.

_____ (2005) An investigation of the relationship between bulk composition, inferred reaction progress and fluid-flow parameters for layered micaceous carbonates from Maine, USA. Journal of Metamorphic Geology, 23, 181-197.

Ferry, J. M. (1976) Metamorphism of calcareous sediments in the Waterville-Vassalboro area, south-central Maine: Mineral reactions and graphical analysis. American Journal of Science, 276, 841-882.

_____ (1978) Fluid interaction between granite and sediment during metamorphism, south-central Maine. American Journal of Science, 278, 1-25-1056.

_____ (1979) A map of chemial potential differences within an outcrop. American Mineralogist, 64, 966-985.

_____ (1980) A case study of the amount and distribution of heat and fluid during metamorphism. Contributions to Mineralogy and Petrology, 71, 373-385.

_____ (1981) Petrology of graphitic sulfide-rich schists from south-central Maine: An example of desulfidation during prograde regional metamorphism. American Mineralogist, 66, 908-930.

_____ (1983) Regional metamorphism of the Vassalboro Formation, south-central Maine, USA: A case study of the role of fluid in metamorphic petrogenesis. Journal of the Geological Society of London, 140, 551-576.

_____ (1984) A biotite isograd in south-central Maine, U.S.A.: Mineral reactions, heat transfer, and fluid transfer. Journal of Petrology, 25, 871-893.

_____ (1987) Metamorphic hydrology at 13-km depth and 400-550 °C. American Mineralogist, 72, 39-58.

_____ (1988) Infiltration-driven metamorphism in northern New England, USA. Journal of Petrology, 29, 1121-1159.

_____ (1992) Regional metamorphism of the Waits River Formation, eastern Vermont: Delineation of a new type of giant metamorphic hydrothermal system. Journal of Petrology, 33, 45-94.

_____ (1994) Overview of the petrologic record of fluid flow during regional metamorphism in northern New England. American Journal of Science, 294, 905-988.

Ferry, J. M., and Gottschalk, M. (2009) The effect of salinity on infiltration-driven contact metamorphism of carbonate rocks. Contributions to Mineralogy and Petrology, 158, 619-636.

Ferry, J. M., Winslow, N. W., and Penniston-Dorland, S. C. (2013) Re-evaluation of infiltration-driven regional metamorphism in northern New England: New transport models with solid solution and cross-layer equilibration of fluid composition. Journal of Petrology, 54, 2455-2485.

Goldschmidt, V. M. (1912) Die Gesetze der Gesteinmetamorphose. Norsk Videnkapsselskaps Skrifter I. Matematisk-Naturvidenskapelig Klasse, 22, 16 p.

Greenwood, H. J. (1963) Metamorphic reactions involving two volatile components. Carnegie Institution of Washington Yearbook, 61, 82-85.

_____ (1967) Mineral equilibria in the system MgO-SiO_2-H_2O-CO_2. In P.H. Abelson,

Ed. Researches in Geochemistry Volume 2, p. 542-567. John Wiley & Sons, New York.

Hanson, R. B. (1992) Effects of fluid production on fluid flow during regional and contact metamorphism. Journal of Metamorphic Geology, 10, 87-97.

_____ (1997) The hydrodynamics of regional metamorphism due to continental collision. Economic Geology, 92, 880-891.

Hewitt, D. A. (1973) The metamorphism of micaceous limestones from south-central Connecticut. American Journal of Science, 273-A, 444-469.

Kerrick, D. M., and Jacobs, G. K. (1981) A modified Redlich-Kwong equation for H_2O, CO_2, and H_2O-CO_2 mixtures at elevated pressures and temperatures. American Journal of Science, 281, 735-767.

Lyubetskaya, T., and Ague, J. J. (2009) Modeling the magnitudes and directions of regional metamorphic fluid flow in collisional orogens. Journal of Petrology, 50, 1505-1531.

_____ (2010) Modeling metamorphism in collsional orogens intruded by magmas: II. Fluid flow and implications for Barrovian and Buchan metamorphism, Scotland. American Journal of Science, 310, 459-491.

Olsen, S. N., and Ferry, J. M. (1995) A comparative fluid inclusion study of the Waterville and Sangerville Formations, south-central Maine. Contributions to Mineralogy and Petrology, 118, 396-413.

Orville, P. M. (1972) Plagioclase cation exchange equilibria with aqueous chloride solutions: Results at 700 °C and 2000 bars in the presence of quartz. American Journal of Science, 272, 234-272.

Osberg, P. H. (1968) Stratigraphy, structural geology, and metamorphism in the Waterville-Vassalboro area, Maine. Maine Geological Survey Bulletin 20.

_____ (1979) Geologic relationships in south-central Maine. In P.H. Osberg and J. W. Skehan, Eds. The Caledonides in the U.S.A., p. 37-62. Weston Observatory of Boston College, Weston, Massachusetts.

_____ (1988) Geologic relations in the shale-wacke sequence in south-central Maine. Maine Geological Survey Studies in Maine Geology, 1, 51-73.

Penniston-Dorland, S. C., and Ferry, J. M. (2006) Development of spatial variations in reaction progress during regional metamorphism of micaceous carbonate rocks, northern New England. American Journal of Science, 306, 475-524.

Rice, J. M. (1977a) Contact metamorphism of impure dolomitic limestone in the Marysville aureole, Montana. American Journal of Science, 277, 1-24.

_____ (1977b) Contact metamorphism of impure dolomitic limestone in the Boulder aureole, Montana. Contributions to Mineralogy and Petrology, 59, 237-259.

Rumble, D., III (1974) Gibbs phase rule and its application to geochemistry. Journal of the Washington Academy of Science, 62, 199-208.

_____ (1978) Mineralogy, petrology, and oxygen isotope geochemistry of the Clough Formation, Black Mountain, western New Hampshire. Journal of Petrology, 19, 317-340.

Rumble, D., III, Oliver, N. H. S., Ferry, J. M., and Hoering, T. C. (1991) Carbon and oxygen isotope geochemistry of chlorite-zone rocks of the Waterville limestone, Maine, U.S.A. American Mineralogist, 76, 857-866.

Rye, R. O., Schuiling, R. D., Rye, D. M., and Jansen, J. B. H. (1976) Carbon, hydrogen, and oxygen isotope studies of the regional metamorphic complex at Naxos, Greece. Geochimica et Cosmochimica Acta, 40, 1031-1049.

Sisson, V. B., and Hollister, L. S. (1990) A fluid-inclusion study of metamorphosed pelitic and

carbonate rocks, south-central Maine. American Mineralogist, 75, 59-70.

Skelton, A. (2011) Flux rates for water and carbon dioxide during greenschist facies metamorphism. Geology, 39, 43-46.

Skelton A. D. L., Graham, C. J., and Bickle, M. J. (1997) Lithological and structural controls on regional 3-D fluid flow patterns during greenschist facies metamorphism of the Dalradian of the SW Scottish Highlands. Journal of Petrology, 36, 563-586.

Taylor, H. P., Jr. (1974) The application of oxygen and hydrogen isotope studies to problems of hydrothermal alteration and ore deposition. Economic Geology, 69, 843-883.

_____ (1977) Water-rock interactions and the origin of H_2O in granitic batholiths. Journal of the Geological Society of London, 133, 509-558.

_____ (1978) Oxygen and hydrogen isotope studies of plutonic granitic rocks. Earth and Planetary Science Letters, 38, 177-210.

Thompson, J. B., Jr., (1982) Reaction space: An algebraic and geometric approach. In J.M. Ferry, Ed., Characterization of Metamorphism through Mineral Equilibria, 10, p. 33-52. Reviews in Mineralogy, Mineralogical Society of America, Chantilly, Virginia.

Tucker, R. D., Osberg, P. H., and Berry, H. N., IV (2001) The geology of part of Acadia and the nature of the Acadian orogeny across central and eastern Maine. American Journal of Science, 2001, 205-260.

Wark, D., and Watson, E. B. (2004) Interdiffusion of H_2O and CO_2 in metamorphic fluids at ≈490-660 °C and 1 GPa. Geochimica et Cosmochimica Acta, 68, 2693-2698.

Wing, B. A., and Ferry, J. M. (2002) Three-dimensional geometry of metamorphic fluid flow during Barrovian regional metamorphism from an inversion of combined petrologic and stable isotopic data. Geology, 30, 639-642.

Wing, B. A., Ferry, J. M., and Harrison, T. M. (2003) Prograde destruction and formation of monazite and allanite during contact and regional metamorphism of pelites: Petrology and geochronology. Contributions to Mineralogy and Petrology, 145, 228-250.

Zhao, Z., and Skelton, A. (2013) Simultaneous calculation of metamorphic fluid fluxes, reaction rates and timescales of fluid-rock interaction using a novel inverse modeling framework. Earth and Planetary Science Letters, 373, 217-227.

FIGURE CAPTIONS

FIGURE 1. Sketch map of the geological setting of the Waterville limestone, Maine (after Osberg 1968, 1979, 1988 and Ferry, 1976, 1980, 1984, 1987). Arrowheads point to the high-grade side of isograds. Sample locations are the same as those of Ferry (1994), Penniston-Dorland and Ferry (2006), and Ferry et al. (2013).

FIGURE 2. Measured and calculated model values of the progress of biotite-forming reaction 1 (ξ_1) in the Waterville limestone along traverses perpendicular to layering. A vertical line through a symbol for a measured value represents ±2 standard deviations based on the statistics of point counting, when larger than the size of the symbol. (**a**) Measured and model values of ξ_1 match exactly in a set of 24 samples collected over a distance of 85 m at location 5. Numbers correspond to the position (in m) along the traverse at which each sample was collected. Samples that correspond to adjacent layers in the same thin section have the same number and are distinguished by different lower case letters (e.g., layers 6a and 6b). Layers collected <1 m apart but are not adjacent have the same number and are distinguished by different capital letters (e.g., 82A and 82B). (**b**) On average, measured values of ξ_1 are smaller in eight samples collected at location 7 than at location 5. (**c**) Model calculations, based on modal and mineral composition

data for the 24 samples from location 5, reproduce the average measured value of ξ_1 at location 7.

FIGURE 3. Schematic representation of the model flow system considered in the transport calculations. Alternating gray and white bands on the front face of the block represent vertical layering in the Waterville limestone (for clarity, gray and white bands are omitted from the top surface of the block). The origin corresponds to location 5 where *T*-*P* conditions are 450 °C and 3500 bars, based on mineral equilibria. Model *T*-*P* conditions at all other spatial points are determined by conditions at the origin, the constant horizontal and vertical *T* gradients, and the constant vertical *P* gradient. Fluid flow is parallel to layering. Model calculations consider vertical, upward directed flow (*z* direction) and horizontal flow in the *x* direction of increasing *T* at the present level of exposure ($z = 0$). Fluid composition is partially homogenized by CO_2-H_2O diffusion across layering; small differences in X_{CO_2} always exist among the layers, however, by prescribing that differences in $\ln K_s$ among layers are the same as those in Table 2 at each point in space and time. Arrowheads point to the spatial coordinates in Figs. 6 – 9.

FIGURE 4. Calculated values of X_{CO_2} in the 24 layers when present measured and computed values of ξ_1 match exactly at location 5 in the model (**a**), and when the average of present measured and model values of ξ_1 match exactly at location 7 in the model (**b**). Circles are exact values of X_{CO_2} defined by layers that contain both reactants and products of reaction 1. Black triangles represent upper and lower bounds corresponding to layers that either contain products but not all reactants (upper bound) or reactants but not all products (lower bound).

FIGURE 5. An example of the interrelationships among ξ_1, $\ln K_s$, and X_{CO_2}, specifically for layer 29c. The calculated relationship between ξ_1 and $\ln K_s$ depends only on mass balance and is independent of P and T. Calculated X_{CO_2}, however, depends on P and T; results are shown for 3500 bars and 450 °C (right-hand vertical axis). The present measured value of $\xi_1 = 1.46$ mol/10^3 cm^3 rock in layer 29c therefore corresponds to present measured $\ln K_s = -1.298$ regardless of P and T but corresponds to $X_{CO_2} = 0.159$ specifically at 3500 bars and 450 °C.

FIGURE 6. Calculated spatial distribution of ξ_1 for five representative layers along two traverses through the model domain, assuming $X^\circ_{CO_2}$ everywhere has a uniform value of 0.159. (**a**) Vertical traverse, parallel to the direction of fluid flow, through location 5 (Figs. 1, 3) with $z = 0$ corresponding to the present level of exposure. (**b**) Horizontal traverse, perpendicular to the direction of fluid flow and parallel to the x coordinate at the present level of exposure ($z = 0$), through locations 5 and 7 (Figs. 1, 3). Although reaction 1 is driven by the disequilibrium flow mechanism, a widespread distribution of coexisting mineral reactants and products is predicted in both the vertical and horizontal dimensions because most mineral reactants and products are solid solutions. The predicted distribution of reactants and products in the horizontal dimension, however, is much smaller than the distance of at least 12.8 km observed in the field.

FIGURE 7. Calculated spatial distributions of ξ_1 in the same format as Fig. 6 except that $X^\circ_{CO_2}$ everywhere has a uniform value of 0.0155 and that the vertical traverse in panel (**a**) is through location 7 (Figs. 1, 3). A widespread distribution of coexisting mineral reactants and products is predicted in both the vertical and horizontal dimensions, but the predicted distribution of reactants and products in the horizontal dimension (**b**) is much smaller than the distance of at least 12.8 km observed in the field.

FIGURE 8. Variation in $X^\circ_{CO_2}$ with horizontal distance coordinate x used in calculations of the spatial distribution of ξ_1 in the model domain with spatially variable $X^\circ_{CO_2}$ (dotted curve). Model calculations used the quadratic fit of $\ln X^\circ_{CO_2}$ against x for $x \geq -12.8$ km (solid curve). A constant value of $X^\circ_{CO_2} = 0.0155$ at $x < -12.8$ km was adopted to reproduce the observed absence of biotite in metacarbonate rocks of the Waterville Formation northeast of location 7.

FIGURE 9. Calculated spatial distribution of ξ_1 along a horizontal traverse, perpendicular to the direction of fluid flow and parallel to layering at the present level of exposure ($z = 0$), assuming a variation in $X^\circ_{CO_2}$ with distance coordinate x as defined in Fig. 8. The format and layers considered are the same as in Figs. 6 and 7. Results reproduce the observations of coexisting mineral reactants and products of reaction 1 in some layers over the 12.8 km distance between locations 5 and 7, no biotite in metacarbonate rocks >0.1 km northeast of location 7, completion of reaction 1 in all layers >1 km southwest of location 5, some layers (like 52) that contain mineral reactants of reaction 1 but no biotite between locations 5 and 7, and the start and completion of reaction 1 at different spatial positions in different layers.

FIGURE 10. Calculated evolution in plagioclase composition in seven layers during reaction 1 using ξ_1 in reference layer 29c as a proxy for time. When layers contain plagioclase with $0.22 < X_{an} < 0.42$, plagioclase compositions cluster in one of two groups because of efficient Ca-Na exchange among infiltrating fluid and nearby layers according to reaction 3. Plagioclase compositions differ significantly between layers when $0.22 < X_{an}$ or $X_{an} > 0.42$ because a_{an} and a_{ab} are fixed, and homogenization of plagioclase composition by Ca-Na interdiffusion among nearby layers is thus impossible.

FIGURE 11. Calculated T-X_{CO_2} conditions (gray area) for equilibrium between reactants and products of reaction 1 in layer 29c. The upper and lower limits of the gray area are defined by conditions at which reaction 1 starts ($\xi = 0$) and goes to completion ($\xi = \xi_{max}$). The red curve is the relation between $X°_{CO_2}$ and both T (left-hand vertical axis) and distance coordinate x (right-hand vertical axis) defined by the equation and curves in Fig. 8. Because the red curve lies within the gray area for values of T and x corresponding to the area of Fig. 1 between locations 5 and 7, the relation between $X°_{CO_2}$ and T (or x) in Fig. 8 could be explained by horizontal fluid flow during metamorphism in the direction of increasing T.

This is a preprint, the final version is subject to change, of the American Mineralogist (MSA)
Cite as Authors (Year) Title. American Mineralogist, in press.
(DOI will not work until issue is live.) DOI: http://dx.doi.org/10.2138/am-2016-5118

Ferry -- Fig. 1

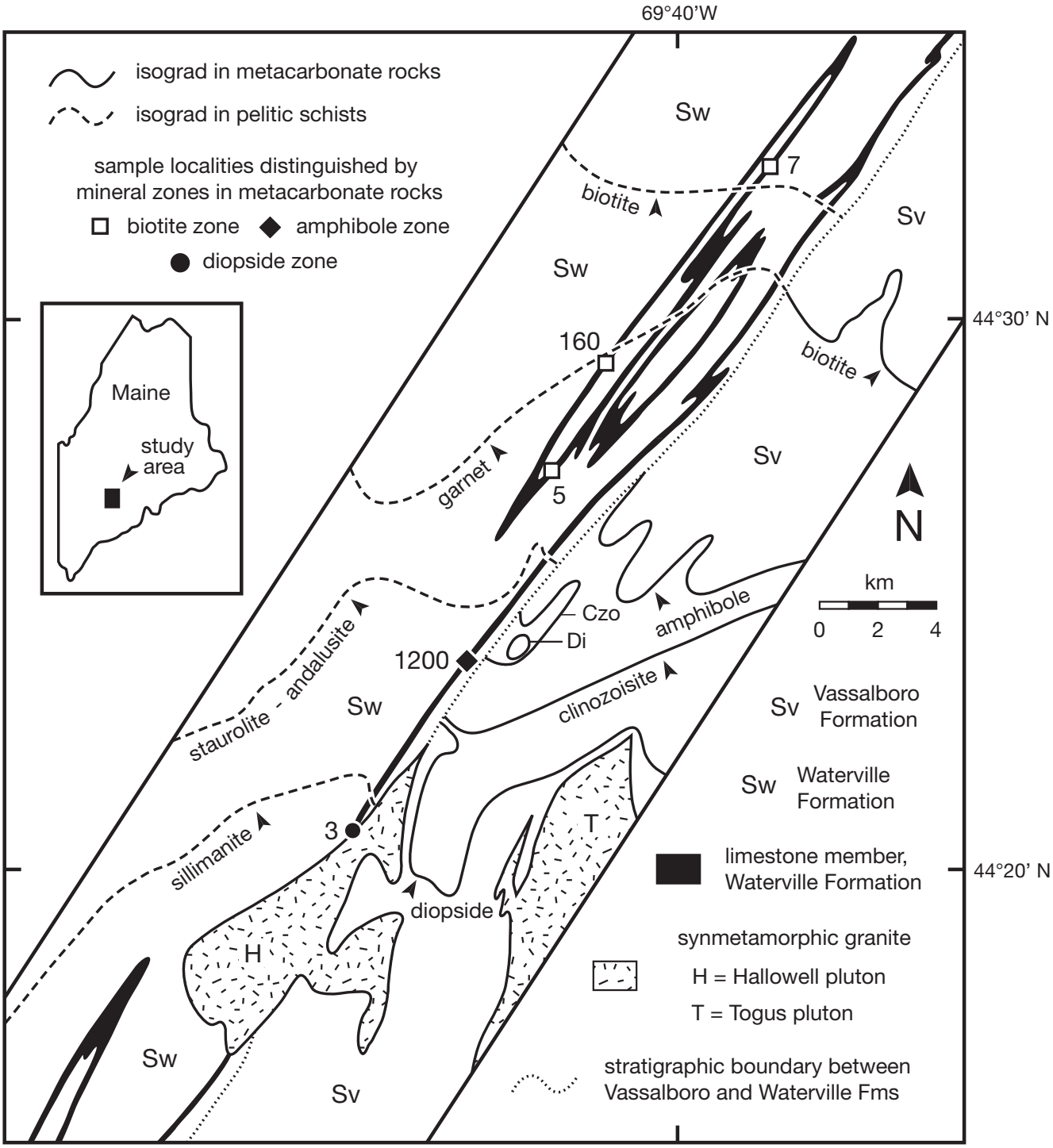

This is a preprint, the final version is subject to change, of the American Mineralogist (MSA)
Cite as Authors (Year) Title. American Mineralogist, in press.
(DOI will not work until issue is live.) DOI: http://dx.doi.org/10.2138/am-2016-5118

Ferry -- Fig. 2

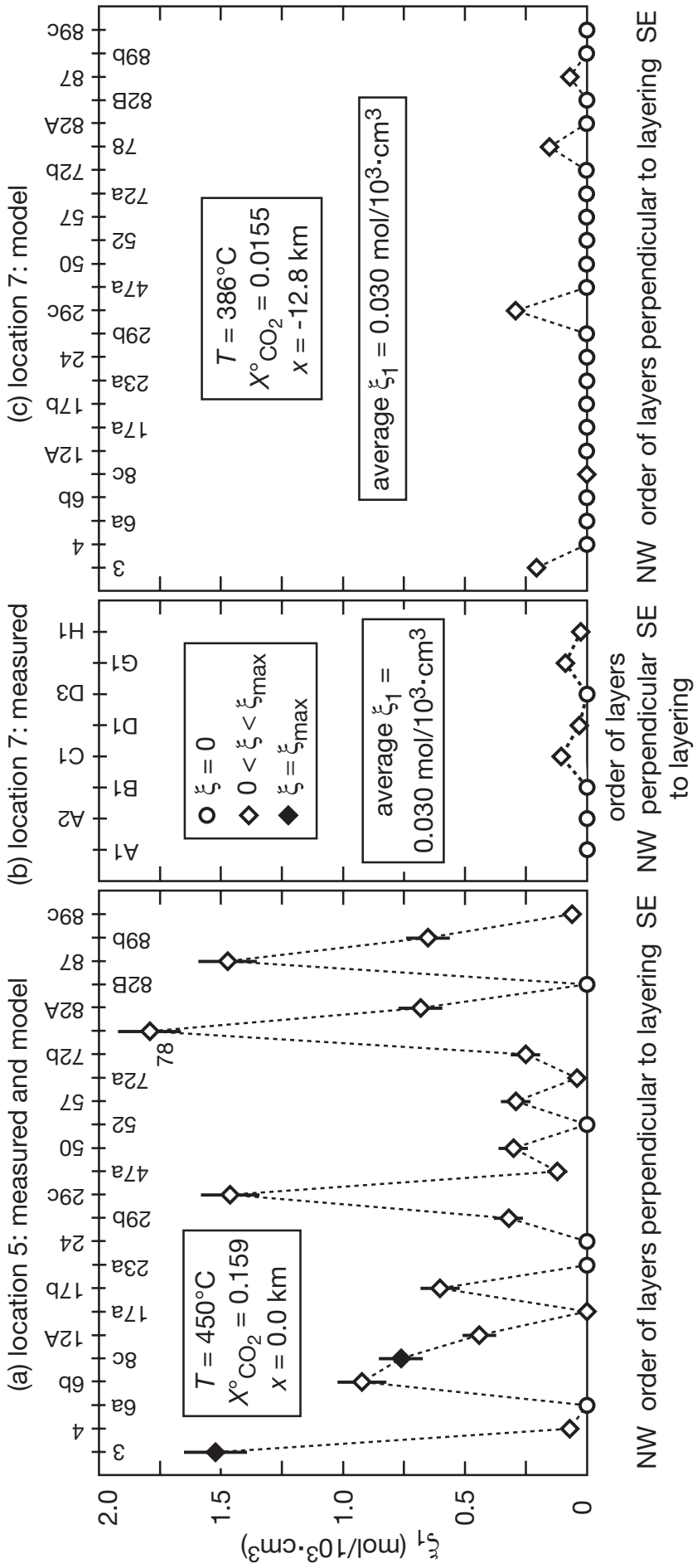

This is a preprint, the final version is subject to change, of the American Mineralogist (MSA)
Cite as Authors (Year) Title. American Mineralogist, in press.
(DOI will not work until issue is live.) DOI: http://dx.doi.org/10.2138/am-2016-5118

Ferry -- Fig. 3

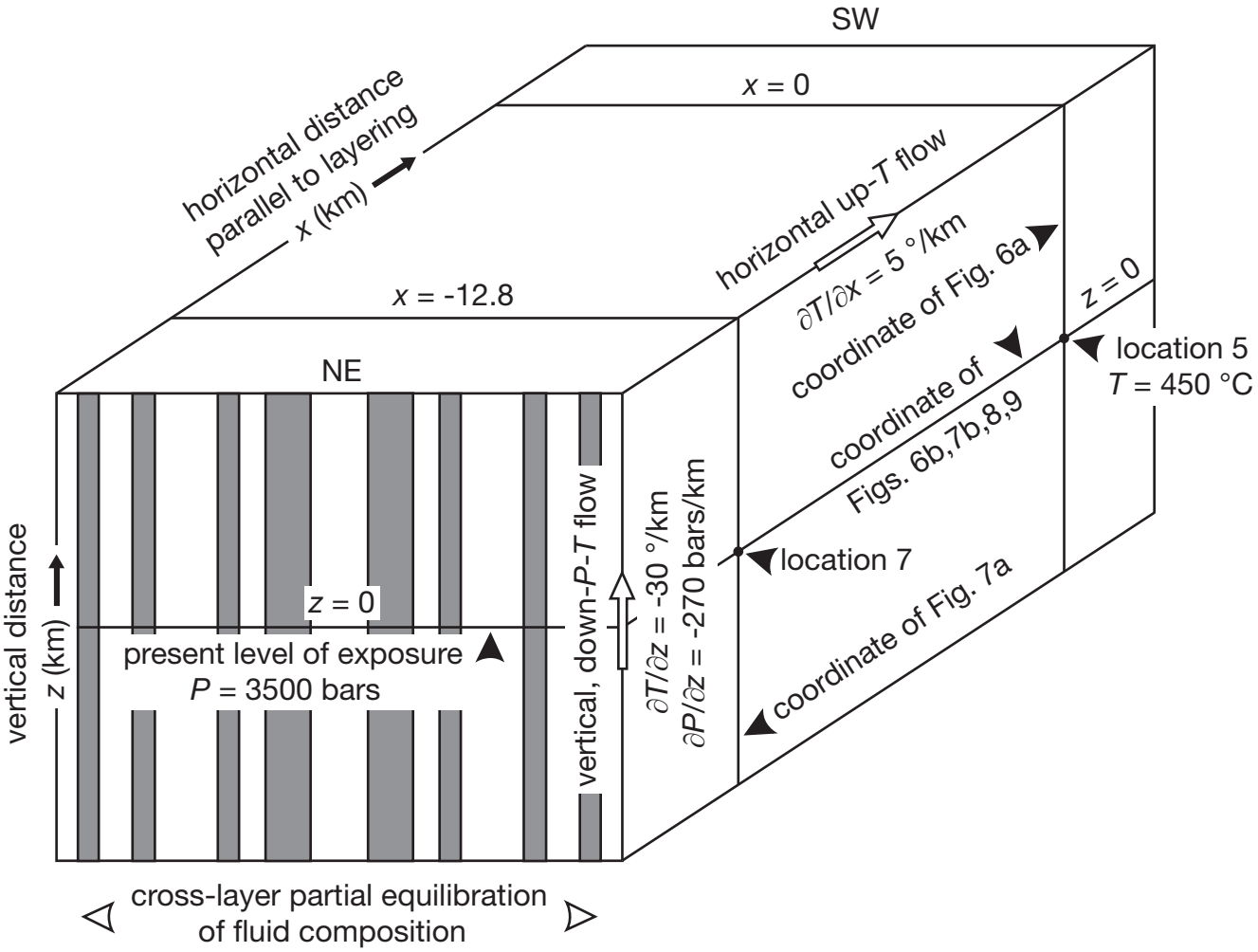

This is a preprint, the final version is subject to change, of the American Mineralogist (MSA)
Cite as Authors (Year) Title. American Mineralogist, in press.
(DOI will not work until issue is live.) DOI: http://dx.doi.org/10.2138/am-2016-5118

Ferry -- Fig. 4

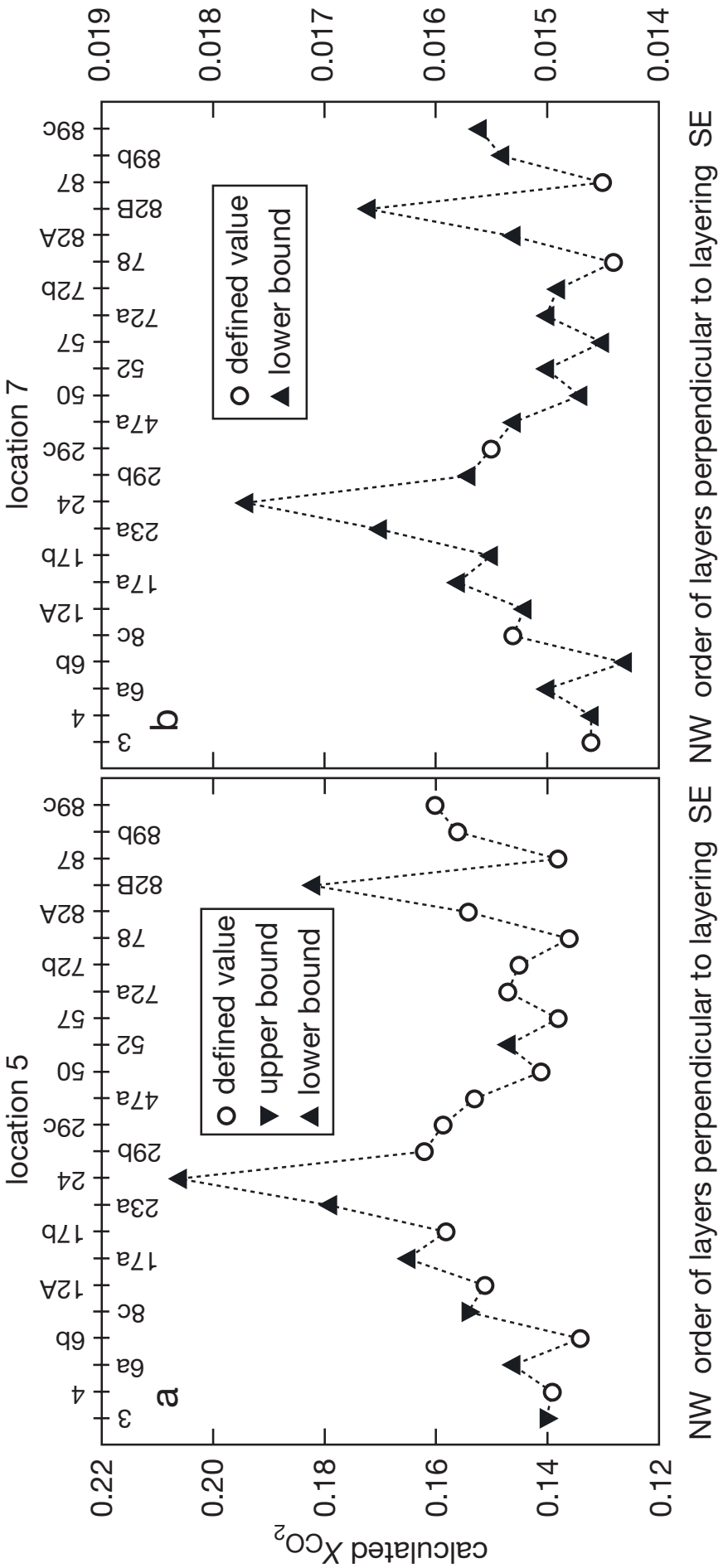

This is a preprint, the final version is subject to change, of the American Mineralogist (MSA)
Cite as Authors (Year) Title. American Mineralogist, in press.
(DOI will not work until issue is live.) DOI: http://dx.doi.org/10.2138/am-2016-5118

Ferry -- Fig. 5

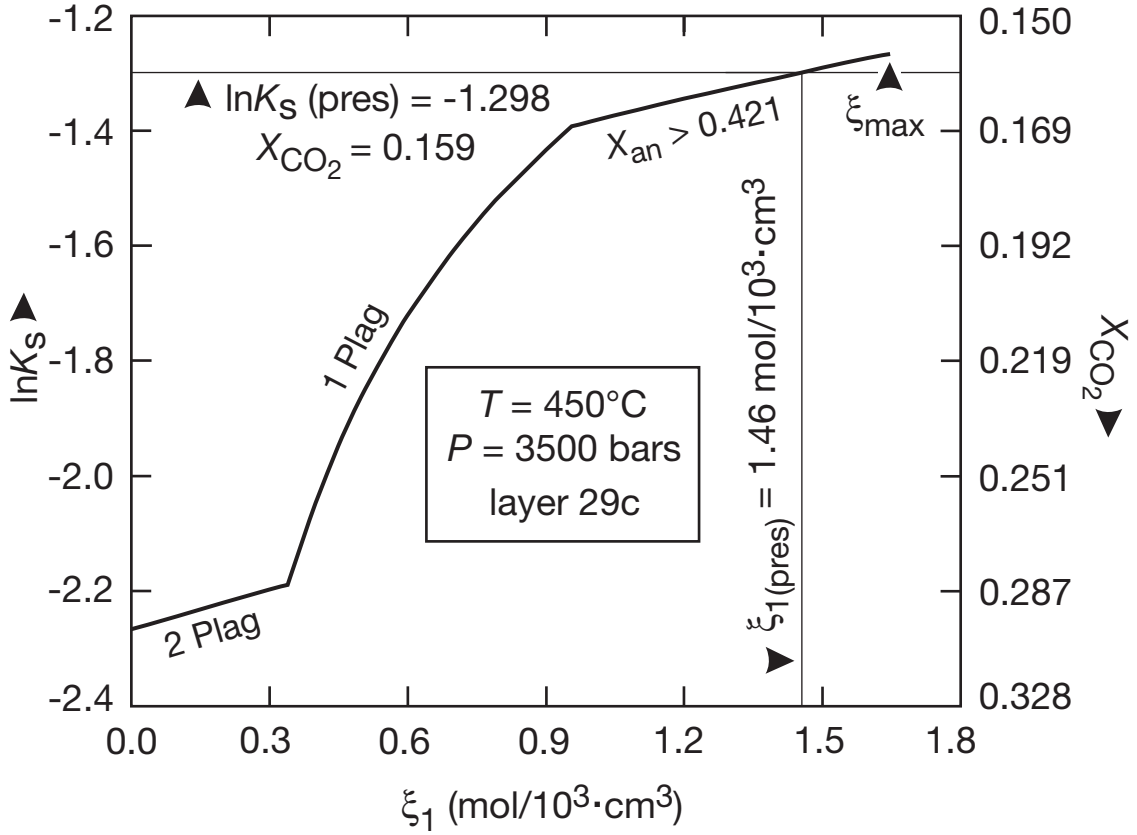

This is a preprint, the final version is subject to change, of the American Mineralogist (MSA)
Cite as Authors (Year) Title. American Mineralogist, in press.
(DOI will not work until issue is live.) DOI: http://dx.doi.org/10.2138/am-2016-5118

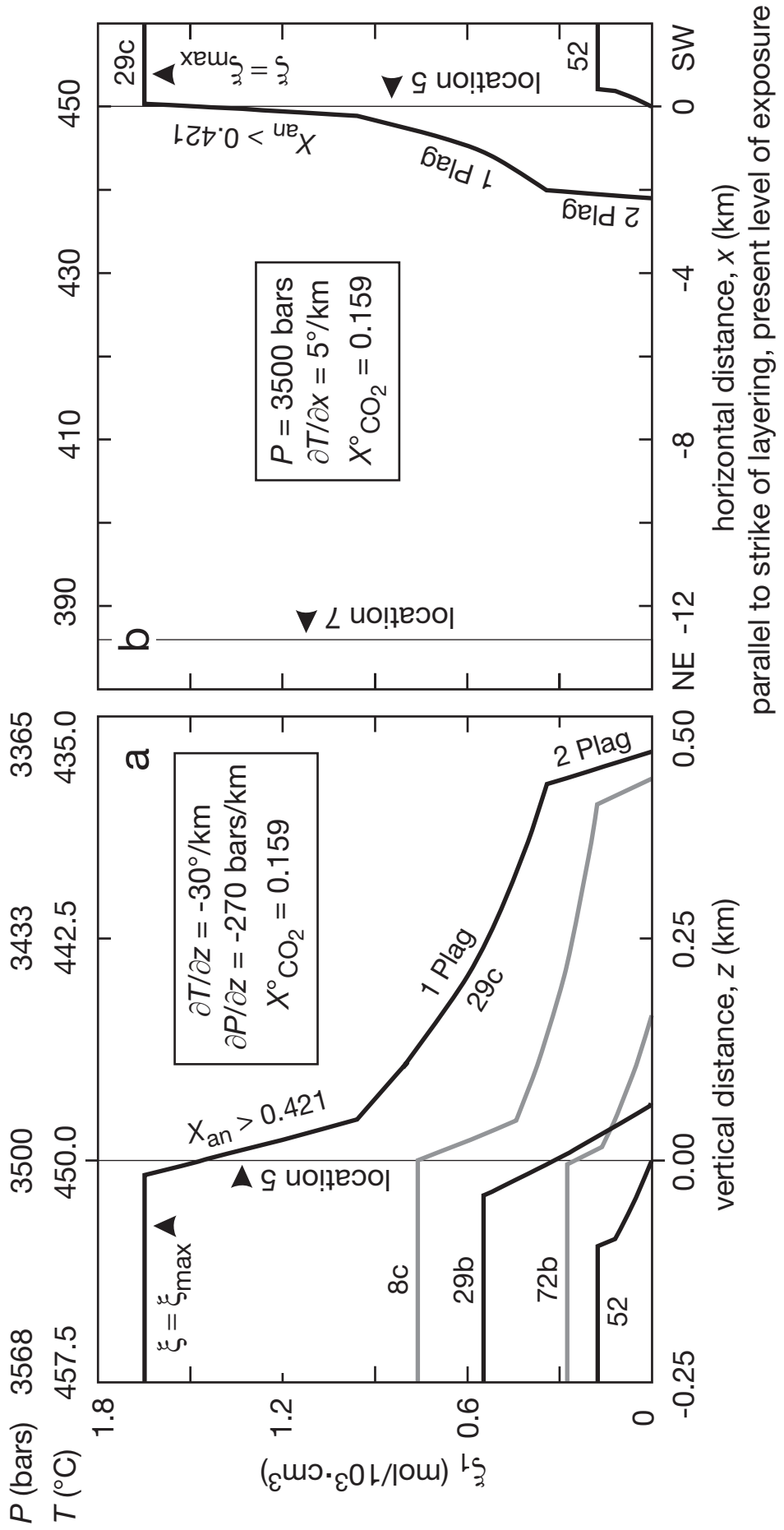

This is a preprint, the final version is subject to change, of the American Mineralogist (MSA)
Cite as Authors (Year) Title. American Mineralogist, in press.
(DOI will not work until issue is live.) DOI: http://dx.doi.org/10.2138/am-2016-5118

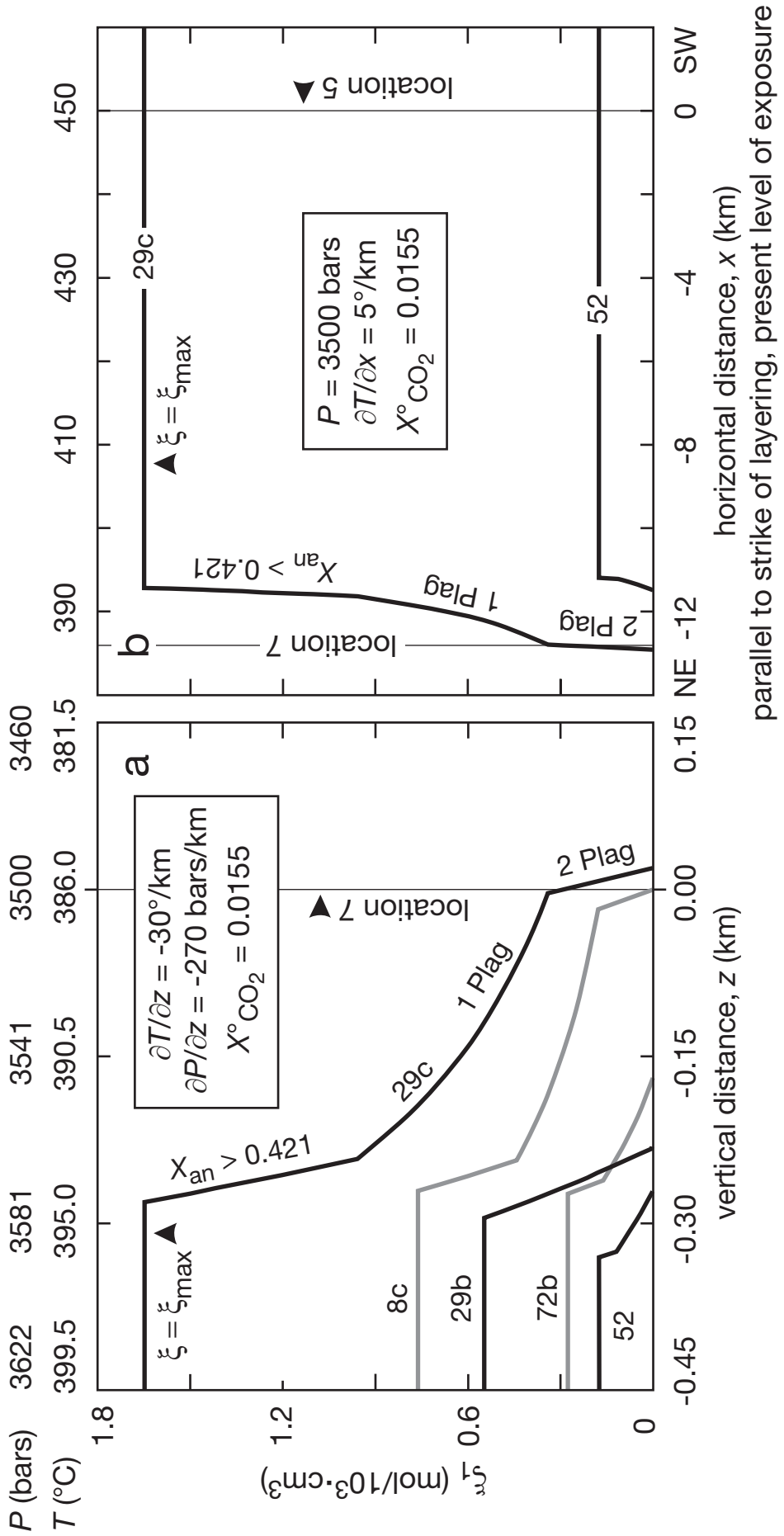

This is a preprint, the final version is subject to change, of the American Mineralogist (MSA)
Cite as Authors (Year) Title. American Mineralogist, in press.
(DOI will not work until issue is live.) DOI: http://dx.doi.org/10.2138/am-2016-5118

Ferry -- Fig. 8

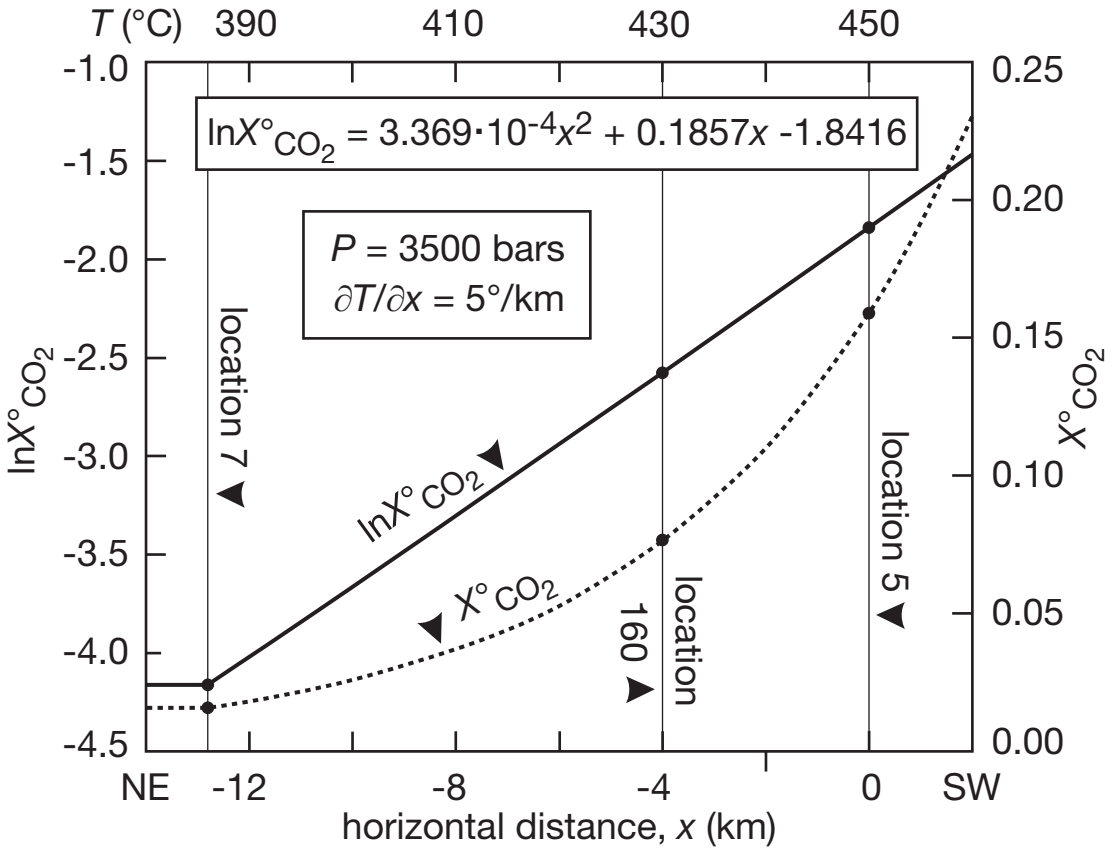

This is a preprint, the final version is subject to change, of the American Mineralogist (MSA)
Cite as Authors (Year) Title. American Mineralogist, in press.
(DOI will not work until issue is live.) DOI: http://dx.doi.org/10.2138/am-2016-5118

Ferry -- Fig. 9

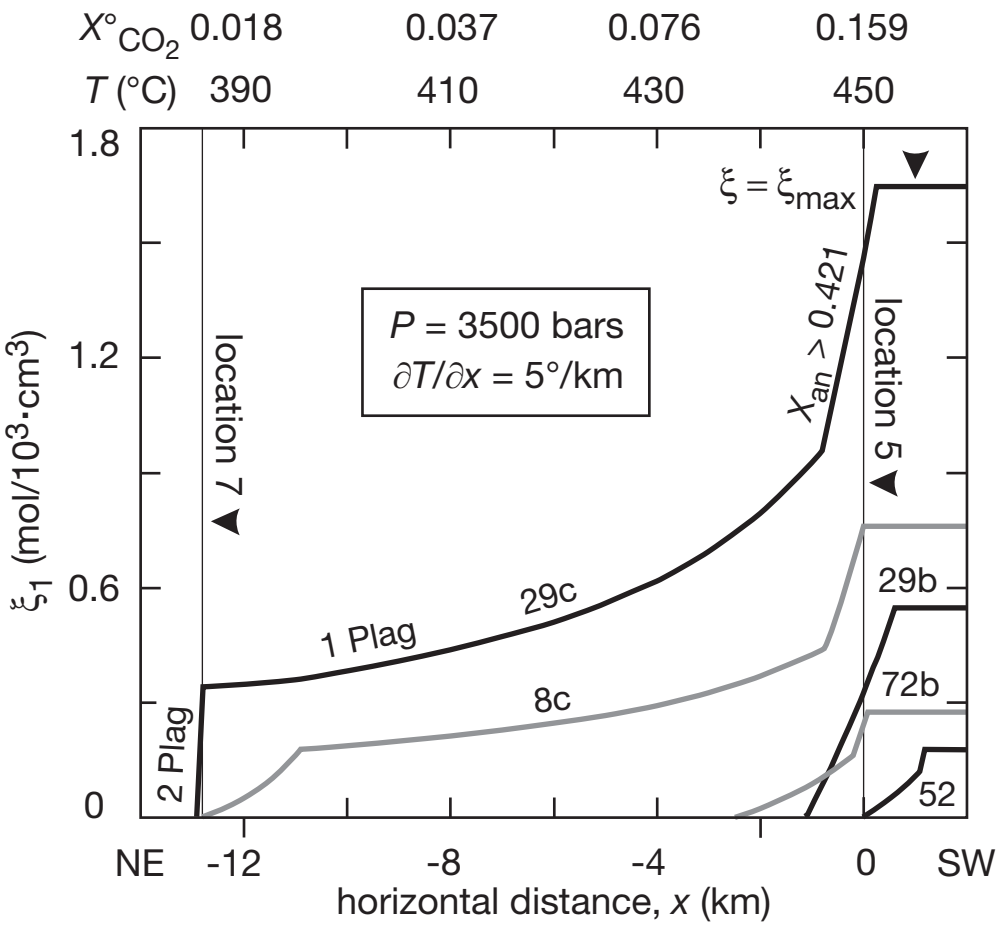

This is a preprint, the final version is subject to change, of the American Mineralogist (MSA)
Cite as Authors (Year) Title. American Mineralogist, in press.
(DOI will not work until issue is live.) DOI: http://dx.doi.org/10.2138/am-2016-5118

Ferry -- Fig. 10

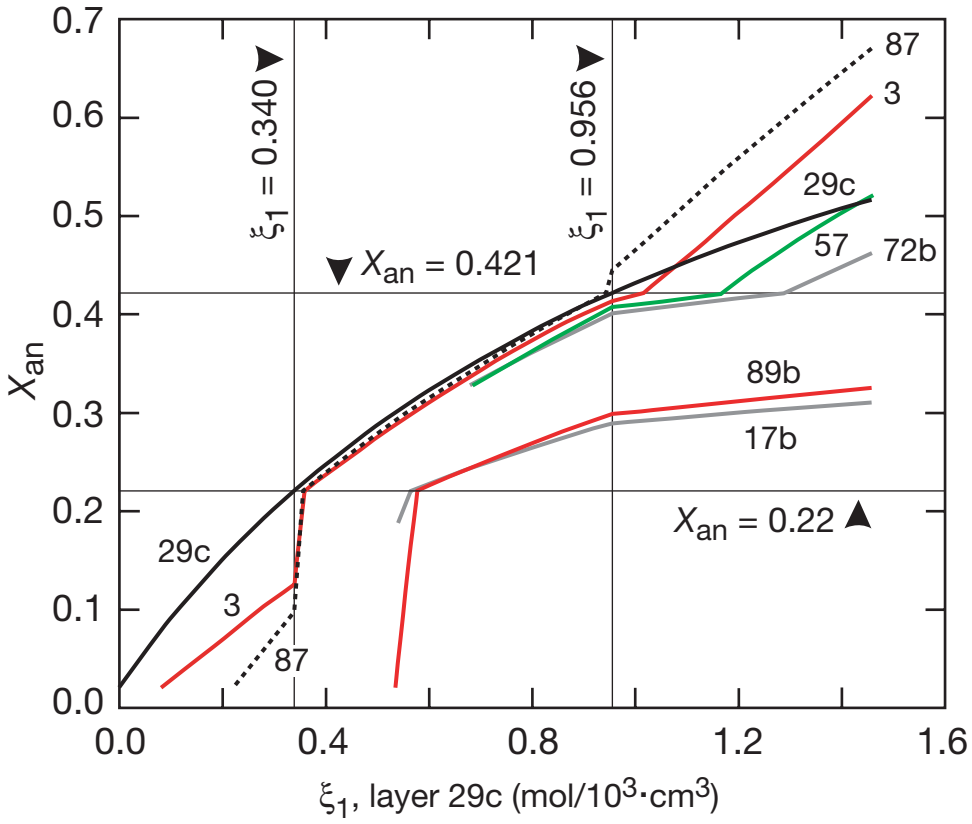

This is a preprint, the final version is subject to change, of the American Mineralogist (MSA)
Cite as Authors (Year) Title. American Mineralogist, in press.
(DOI will not work until issue is live.) DOI: http://dx.doi.org/10.2138/am-2016-5118

Ferry -- Fig. 11

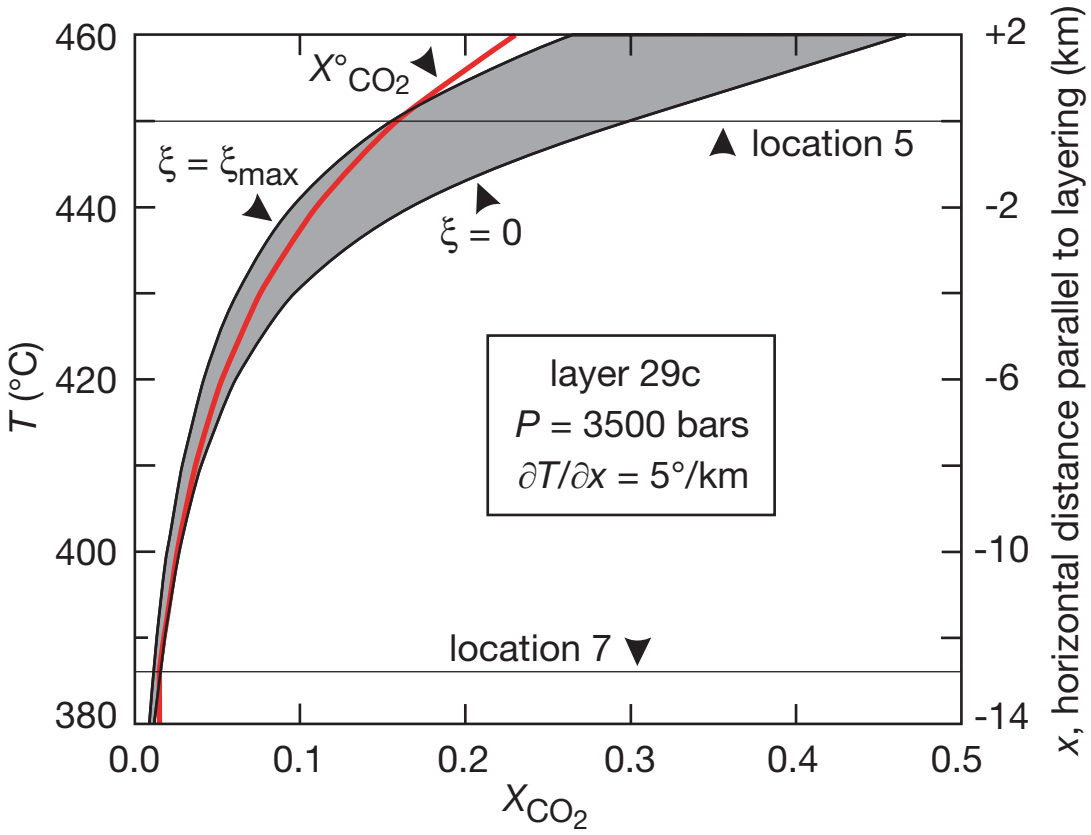

This is a preprint, the final version is subject to change, of the American Mineralogist (MSA)
Cite as Authors (Year) Title. American Mineralogist, in press.
(DOI will not work until issue is live.) DOI: http://dx.doi.org/10.2138/am-2016-5118

TABLE 1A. Average mineral formulas[a]

Mineral (symbol)	Formula
Muscovite (Ms)	$K_{0.91}Na_{0.05}(Mg,Fe)_{0.20}Ti_{0.03}Al_{2.65}Si_{3.14}O_{10}(OH)_2$
Ankerite (Ank)	$Ca_{1.02}(Mg,Fe)_{0.98}(CO_3)_2$
Biotite (Bt)	$K_{0.89}Na_{0.01}(Mg,Fe)_{2.38}Ti_{0.08}Al_{1.57}Si_{2.83}O_{10}(OH)_2$
Calcite (Cal)	$Ca_{0.94}(Mg,Fe)_{0.06}(CO_3)$
Chlorite (Chl)	$(Mg,Fe)_{4.56}Al_{2.65}Si_{2.73}O_{10}(OH)_8$

TABLE 1B. Net-transfer reactions[b]

Number	Reaction
1	0.978 Mg-Ms + 2.353 Mg-Ank + 0.858 Qtz + 0.051 Rt + 0.022 H_2O = 1.000 Mg-Bt + 2.031 Mg-Cal + 0.491 an + 0.039 ab + 2.675 CO_2
2	5.077 Mg-Ank + 0.080 Qtz + 1.325 an + 4.000 H_2O = 1.000 Mg-Chl + 6.918 Mg-Cal + 3.236 CO_2
3	2 ab + $CaCl_2$ = an + 4 Qtz + 2 NaCl

TABLE 1C. Average Fe-Mg exchange coefficients[c]

Coefficient	Average value
$K_{Bt/Ank}$	2.17(0.20)
$K_{Cal/Ank}$	2.14(0.24)
$K_{Ms/Ank}$	2.10 (0.19)
$K_{Chl/Ank}$	1.90(0.21)

[a]Average is of all analyses of a given mineral in the 24 samples from the 100-m traverse at location 5.

[b]Mg-Ms, Mg-Ank, Mg-Bt, Mg-Cal, and Mg-Chl refer to the Mg components of muscovite, ankerite, biotite, calcite, and chlorite (Table 1A); Rt refers to TiO_2 in rutile; Qtz refers to SiO_2 in quartz; and an and ab refer to $CaAl_2Si_2O_8$ and $NaAlSi_3O_8$ components in plagioclase.

[c]$K_{i/Ank} = [(Fe/Mg)_i/(Fe/Mg)_{Ank}] = [(X_{Fei})/(1-X_{Fei})]/[(X_{FeAnk})/(1-X_{FeAnk})]$,where i is biotite, calcite, muscovite, and chlorite, and $X_{Fei} = Fe/(Fe+Mg)_i$. Average is of analyses of all coexisting mineral pairs in the 24 samples from the 100-m traverse at location 5. Standard deviation in parentheses.

TABLE 2. Values of reaction progress, mineral compositions, and related variables used in transport calculations

Layer[a]	X_{an}(pres)[b]	ξ_1(pres)[c] (mol/L)	ξ_1(max)[c] (mol/L)	ξ_3(pres)[d] (mol/L)	$X_{FeAnk}(0)$[e]	$n_{Pl}(0)$[f] (mol/L)	lnK_s(pres)[g]	ln$K_s(0)$[g]	lnK_s(max)[g]	ΔlnK_s[h]
3	0.622	1.52(0.13)	1.520	0.540	0.256	1.799	–1.077	–2.027	–1.077	0.221
4	0.415	0.07(0.03)	0.321	0.295	0.153	0.803	–1.040	–1.128	–0.979	0.237
6a	0.375	0	0.106	0.202	0.146	0.581	–1.154	–1.154	–1.017	0.144
6b	0.435	0.92(0.10)	1.012	0.166	0.192	1.068	–0.996	–1.849	–0.982	0.302
8c	0.581	0.76(0.09)	0.760	0.056	0.301	0.367	–1.242	–2.145	–1.242	0.056
12A	0.489	0.44(0.07)	0.463	0.266	0.263	0.763	–1.211	–1.485	–1.203	0.087
17a	0.302	<0.01(<0.01)	0.287	0.249	0.146	0.900	–1.366	–1.366	–1.056	–0.069
17b	0.310	0.60(0.08)	0.708	0.225	0.171	1.372	–1.288	–1.787	–1.214	0.010
23a	0.294	0	0.254	0.247	0.186	0.921	–1.512	–1.512	–1.194	–0.214
24	0.226	0	0.218	0.303	0.168	1.500	–1.748	–1.748	–1.469	–0.450
29b	0.540	0.32(0.06)	0.545	0.182	0.293	0.464	–1.333	–1.463	–1.257	–0.036
29c	0.516	1.46(0.12)	1.648	0.002	0.348	0.552	–1.298	–2.266	–1.266	0.000
47a	0.409	0.12(0.04)	0.158	0.166	0.220	0.507	–1.229	–1.424	–1.185	0.069
50	0.408	0.30(0.06)	0.481	0.218	0.173	0.756	–1.085	–1.404	–1.020	0.213
52	0.363	0	0.174	0.156	0.138	0.464	–1.160	–1.160	–0.970	0.138
57	0.521	0.29(0.06)	0.361	0.083	0.178	0.275	–1.050	–1.376	–1.031	0.248
72a	0.508	0.04(0.02)	0.058	0.100	0.190	0.233	–1.159	–1.177	–1.151	0.139
72b	0.461	0.25(0.06)	0.276	0.119	0.207	0.394	–1.133	–1.463	–1.125	0.165
78	0.516	1.79(0.13)	1.834	0.085	0.231	0.931	–1.026	–1.957	–1.021	0.272
82A	0.309	0.68(0.09)	1.094	–0.061	0.152	0.388	–1.248	–1.730	–1.003	0.049
82B	0.254	0	0.323	0.258	0.140	1.125	–1.532	–1.532	–1.182	–0.235
87	0.670	1.47(0.12)	1.608	0.249	0.233	0.899	–1.047	–1.965	–1.030	0.251
89b	0.325	0.65(0.09)	0.944	0.229	0.166	1.579	–1.265	–1.774	–0.987	0.033
89c	0.329	0.06(0.03)	0.256	0.183	0.163	0.657	–1.310	–1.411	–1.067	–0.012

[a]Same as sample numbers in Penniston-Dorland & Ferry (2006) and Ferry et al. (2013).
[b]Present average measured plagioclase composition.
[c]Present measured and calculated maximum possible progress of reaction 1 in mol/10^3·cm^3. Uncertainties in present measured values in parentheses are 2 standard deviations based on the statistics of point counting (Chayes, 1956).

[d]Progress of reaction (3), in mol/10^3·cm^3, that with initial composition and amount of plagioclase gives the present average X_{an} when $\xi_1 = \xi_1$(pres).
[e]Calculated Fe/(Fe+Mg) of ankerite at the start of reaction 1.
[f]Calculated initial amount of plagioclase at the start of reaction 1 in mol/10^3·cm^3.
[g]lnK_s(pres): value computed from present measured mineral compositions; lnK_s(0): value at the start of reaction (1); lnK_s(max): value when reaction (1) is complete at the maximum possible value of ξ_1.
[h]$\Delta \ln K_s$ = [lnK_s(pres) for each layer] – [lnK_s(pres) for layer 29c].